



Universitat Autònoma de Barcelona

ADVERTIMENT. L'accés als continguts d'aquesta tesi queda condicionat a l'acceptació de les condicions d'ús establertes per la següent llicència Creative Commons:  http://cat.creativecommons.org/?page_id=184

ADVERTENCIA. El acceso a los contenidos de esta tesis queda condicionado a la aceptación de las condiciones de uso establecidas por la siguiente licencia Creative Commons:  <http://es.creativecommons.org/blog/licencias/>

WARNING. The access to the contents of this doctoral thesis it is limited to the acceptance of the use conditions set by the following Creative Commons license:  <https://creativecommons.org/licenses/?lang=en>



Universitat Autònoma
de Barcelona

**Human prostaglandin reductase 1 (PTGR1):
Substrate specificity, site-directed mutagenesis and
catalytic mechanism**

Thesis dissertation presented by **Julio Mesa Solís**, in partial fulfillment of the requirements for the degree of Ph.D. in Biochemistry, Molecular Biology and Biomedicine.

The work was performed at the Department of Biochemistry and Molecular Biology in the Universitat Autònoma de Barcelona, under the direction of doctors **Xavier Parés Casasampera, Jaume Farrés Vicén and Sergio Porté Orduna**.

Xavier Parés Casasampera

Jaume Farrés Vicén

Sergio Porté Orduna

Bellaterra, June 9, 2016

Front:

Ribbon representation of the Human Prostaglandin Reductase 1 homodimer with bound NADP⁺, using the PyMOL program. PDB code 2Y05

Back Cover:

Stick representation of Prostaglandin atomic structure. Oxygen atoms depicted in red

Top: 15-*keto*-Prostaglandin E₂

Down: 15-Deoxy- $\Delta^{12,14}$ -Prostaglandin J₂

Agradecimientos

Llego al punto final de esta apasionante etapa y sin duda me hubiera resultado completamente imposible si no fuera por el gran apoyo que he recibido de una infinidad de personas. Desgraciadamente no podré nombrar a todos y cada uno de ellos, pero no quisiera dejar pasar por alto las que fueron claves durante este proceso.

En primer lugar, me gustaría dar las gracias a mis padres, desde siempre fomentaron y potenciaron mi educación. Me proporcionaron un ambiente idóneo donde desarrollar mis conocimientos y siempre dejaron que yo decidiera el camino a seguir, apoyándome ciegamente al confiar en mi criterio. Ellos tal vez no lo sepan, pero si he llegado hasta aquí es sin duda culpa suya. Estoy seguro de que, si ellos hubieran tenido las mismas oportunidades que yo he tendido, ambos serían unos magníficos científicos, ya que tienen todas las cualidades necesarias para serlo.

En segundo lugar, quisiera agradecerle a mi hermana haber aguantado a su hermano. Me hacías ver que si era difícil era porque valía la pena. Tenías razón, es lo más difícil intelectualmente que he hecho y me siento tremendamente orgulloso.

Pero si hay una culpable de que haya hecho el Doctorado, esa es mi queridísima mujer. Mayra, tú tienes la culpa de que decidiera hacer un Máster en Bioquímica, Biología Molecular y Biomedicina, el mismo que me abrió la puerta un año más tarde a este viaje tan intenso y enriquecedor. Gracias mi amor, por hacerme mirar hacia las estrellas para poder llegar mucho más lejos de lo que jamás me había planteado.

Sin duda, el cambio de estar trabajando como técnico de laboratorio a hacerlo como personal de investigación en formación fue muy significativo. Afortunadamente tuve grandísimos apoyos en forma de dos personas claves. La primera fue Agrin, paciente conmigo en mis primeros compases en este mundo nuevo. Me diste confianza para saber que claro que lo podía hacer y, lo más importante, me transmitiste tu ilusión y tus ganas de aprender más y más. La segunda persona, más que un apoyo, fue un pilar central de esta Tesis, sin él sencillamente no habría Tesis. Sergio, gracias por tus sugerencias, consejos y por todo el tiempo que has invertido en mi formación.

Mis queridos compañeros ADHs: Cristina, Raquel, Joan e Isidro. Sin vosotros todo hubiera sido más largo y aburrido. Me enorgullece el magnífico compañerismo que siempre hubo entre nosotros. Habéis sido los compañeros ideales de viaje y quisiera daros las gracias por todos los buenos momentos vividos y sobre todo por estar ahí también cuando un resultado no sale como te esperabas, es decir, casi todo el tiempo en ciencia.

Durante estos años han sido muchos los que como yo pasábamos muchísimas horas en la Torre C2. Catedráticos, profesores, técnicos, futuros investigadores... y de entre ellos quisiera destacar a dos. Chari, he aprendido muchísimo de ti, quisiera agradecerte todo el tiempo que me has dedicado. Aunque nunca fue oficial, siempre fuiste uno de mis directores de Tesis. Helena, mi querida Helena, gracias por tu apoyo en el laboratorio y sobre todo, gracias por tu apoyo fuera de él. Como le dijo a mi mujer, pon una Helena en tu vida y todo será más fácil.

La presente Tesis incluye un capítulo donde fueron realizados espectros de RMN. Gracias a la colaboración de los Doctores Carles Jaime y Albert Virgili, fue posible llegar a una detallada interpretación de los mismos, motivo por el cual les estoy inmensamente agradecido.

Como miembros de mi comisión de seguimiento, tuve el honor de contar con tres magníficos investigadores, la Dra. M. Victòria Nogués, la Dra. Irantzu Pallarès y el Dr. Oriol Gallego, que supieron orientarme a lo largo de los cuatro años, me dieron valiosos consejos y supieron poner el foco siempre en lo importante para que no me perdiera en los detalles.

Asimismo quisiera dar las gracias a los Doctores Xavier Parés y Jaume Farrés. Me dieron la oportunidad de estar en su grupo y confiaron en mis cualidades como científico junior antes de que yo mismo supiera que las tenía. Siempre tuvieron la puerta de su despacho abierta y, sin sus gestiones y correcciones, esta Tesis no hubiera sido posible.

Durante el desarrollo de la presente Tesis, he crecido intelectualmente y sobre todo he hecho un sinfín de nuevos amigos. Empezando por toda la gente de la Unidad de Bioquímica de Biociencias de la UAB, pasando por otros departamentos de esta misma universidad y llegando incluso a Estados Unidos, donde fui acogido en el laboratorio del Prof. M.G. Finn (School of Chemistry and Biochemistry, Georgia Tech). No es posible nombraros a todos, afortunadamente sois demasiados, pero quisiera que sepáis cuánto me habéis ayudado en este proceso. Gracias a todos de corazón.

Sería imposible haber realizado todo este trabajo sin el apoyo económico adecuado, por lo que también quisiera agradecer haber obtenido

una beca PIF, otra beca de apoyo para el aprendizaje de lenguas extranjeras y una beca final de movilidad, todas ellas otorgadas por la Universitat Autònoma de Barcelona. Finalmente, agradezco la financiación recibida para el desarrollo del proyecto por el Ministerio de Economía y Competitividad (BFU2011-24176) y la Generalitat de Catalunya (2009 SGR 795).

Abstract

The work here presented is part of the structural and functional characterization of the protein superfamily of medium-chain dehydrogenases/reductases (MDRs), which can be divided into two main groups: Zn-dependent and Zn-independent MDRs. In order to contribute to the knowledge on Zn-independent MDRs, our group previously published several reports on ζ -crystallin and p53-inducible gene 3 (PIG3) protein. Here we have extended this endeavor now featuring prostaglandin reductases (PTGRs), a group of proteins belonging to the alkenal/one oxidoreductase (AOR) protein family. The physiological substrates of PTGRs, prostaglandins (PGs), are lipid compounds derived from arachidonic acid by the action of cyclooxygenases, acting locally as messenger molecules in a wide variety of physiological processes, such as inflammation, cell survival, apoptosis, smooth muscle contraction, adipocyte differentiation, vasodilation and platelet aggregation inhibition. In the inactivating pathway of PGs, the first metabolic intermediates are 15-*keto*-PGs, which are further converted into 13,14-dihydro-15-*keto*-PGs by different enzymes having 15-*keto*-PG reductase activity. Three human PTGRs, Zn-independent members of the MDR superfamily, perform the first irreversible step of the degradation pathway.

The first chapter is focused on the characterization of the recombinant human PTGR1, also known as leukotriene B₄ dehydrogenase. Only a partial characterization of this enzyme, isolated from human placenta, had been previously reported. In the present work, we have performed an extensive kinetic characterization of PTGR1, which catalyzes

the NADPH-dependent reduction of the α,β -double bond of aliphatic and aromatic aldehydes and ketones, and 15-*keto*-PGs. PTGR1 also shows low activity in the oxidation of leukotriene B₄. The best substrates in terms of k_{cat}/K_m were 15-*keto*-PGE₂, *trans*-3-nonen-2-one and *trans*-2-decenal. We develop a more reliable and sensitive methodology to detect PG derivatives at submicromolar concentrations. The newly devised HPLC-based method uses end-point analysis of the reaction products for measuring the enzymatic activity of PTGRs and has been applied successfully to the subsequent kinetic studies with 15-*keto*-PGs and 15-deoxy- $\Delta^{12,14}$ -prostaglandin J₂ (15d-PGJ₂). Molecular docking simulations, based on the three-dimensional structure of the human enzyme (PDB ID 2Y05), and site-directed mutagenesis studies were performed to pinpoint important structural determinants, highlighting the role of Arg56 and Tyr245 in 15-*keto*-PG binding. Finally, inhibition analysis was done using non-steroidal anti-inflammatory drugs (NSAIDs) as potential inhibitors.

The second chapter is centered on the activity of PTGR1 with 15d-PGJ₂, which is a natural ligand of peroxisome proliferator-activated receptor gamma and a highly reactive electrophilic molecule. Some of the biological effects of 15d-PGJ₂ are mediated through receptor-independent pathways relying on posttranslational protein modification. Inactivation of 15d-PGJ₂ can be achieved by double-bond hydrogenation catalyzed by AORs, such as PTGR1. By using ¹H and ¹³C NMR spectroscopy, we have identified two different diastereoisomers, (12*R*)- and (12*S*)-12,13-dihydro-15d-PGJ₂, as the products of human PTGR1 activity, proving the enzymatic hydrogenation of the C12-C13 α,β -double bond. Molecular docking of 15d-PGJ₂ into the crystallographic structure of human PTGR1 predicts three tyrosine residues

(Tyr49, Tyr245 and Tyr273) making van der Waals interactions with the substrate and a properly positioned C β atom for hydride transfer from the C4 atom of the NADPH nicotinamide. However, Tyr49 is not well oriented while substitution of either Tyr245 or Tyr273 by site-directed mutagenesis yields active enzyme, thus discarding their participation as proton donor residues. Considering these results, we propose a catalytic mechanism where the NADPH hydride first attacks the electrophilic C13 atom, and then protonation of the C12 atom takes place with little stereoselectivity. Since a suitably positioned proton donor residue is not available, a solvent proton could be added from both substrate faces, leading to the formation of the two diastereomeric products. The here described mechanism is also fully compatible with the hydrogenation of the C13-C14 double bond of 15-keto-PGs by PTGR1.

Index

| | |
|---|-----------|
| Abbreviations | 19 |
| 1. General Introduction | 21 |
| 1.1. Medium-chain Dehydrogenases/Reductases | 23 |
| 1.2. Zn-independent MDRs | 25 |
| 1.3. Alkenal/one oxidoreductases | 27 |
| 1.4. Prostaglandin reductase 1 (PTGR1) | 28 |
| 1.5. Prostaglandin reductase 2 and 3 | 33 |
| 1.6. Catalytic and kinetic mechanisms of PTGRs | 34 |
| 1.7. Physiological role of PTGRs | 37 |
| 1.7.1. Prostaglandins (PGs) | 37 |
| 1.7.2. PTGRs and cancer | 41 |
| 1.8. Enoyl thioester reductases | 43 |
| 2. Objectives | 45 |
| 3. Chapter 1: Human prostaglandin reductase 1 (PTGR1): Substrate specificity, inhibitor analysis and site-directed mutagenesis | 49 |
| 3.1. Abstract | 51 |
| 3.2. Introduction | 53 |
| 3.3. Materials and methods | 56 |
| 3.3.1. Protein expression and purification | 56 |
| 3.3.2. Cofactor binding to PTGR1 by quenching of intrinsic fluorescence | 57 |

| | |
|---|----|
| 3.3.3. Molecular weight determination by gel filtration-HPLC analysis | 58 |
| 3.3.4. Kinetic characterization with α,β -unsaturated aldehydes and ketones | 58 |
| 3.3.5. Kinetic characterization with prostaglandins and LTB ₄ by a novel HPLC-based method | 59 |
| 3.3.6. Determination of the IC ₅₀ value for putative PTGR1 inhibitors | 60 |
| 3.3.7. Docking simulations | 60 |
| 3.4. Results | 62 |
| 3.4.1. New HPLC-method for determination of 15- <i>keto</i> prostaglandin reductase activity | 62 |
| 3.4.2. Cofactor specificity of human PTGR1 and quaternary structure | 66 |
| 3.4.3. Kinetic characterization of human PTGR1 with α,β -unsaturated aldehydes and ketones | 70 |
| 3.4.4. Kinetic characterization of human PTGR1 with prostaglandins and LTB ₄ through a new HPLC-based method | 70 |
| 3.4.5. Docking simulations of 15- <i>keto</i> -prostaglandin E ₂ to PTGR1 | 76 |
| 3.4.6. Kinetic characterization of human PTGR1 mutants Agr56Ala, Tyr245Phe and Tyr245Ala | 79 |
| 3.4.7. Inhibition of human PTGR1 by classical inhibitors of Prostaglandin metabolism | 80 |
| 3.4.8. Docking simulations of indomethacin and niflumic acid to PTGR1 | 82 |

| | |
|--|-----|
| 3.5. Discussion | 86 |
| 4. Chapter 3: Carbon-carbon double-bond hydrogenation of 15-deoxy- $\Delta^{12,14}$ -prostaglandin J ₂ by human prostaglandin reductase 1: Product identification by ¹ H and ¹³ C NMR spectroscopy and catalytic mechanism | 91 |
| 4.1. Abstract | 93 |
| 4.2. Introduction | 95 |
| 4.3. Material and methods | 97 |
| 4.3.1. Materials | 97 |
| 4.3.2. Site-directed mutagenesis | 97 |
| 4.3.3. Protein expression and purification | 98 |
| 4.3.4. Kinetic characterization by HPLC-based method | 99 |
| 4.3.5. Docking simulations | 100 |
| 4.3.6. NMR analysis of PTGR1 reactions products | 101 |
| 4.4. Results and discussion | 102 |
| 4.4.1. NMR analysis of human PTGR1 activity with 15d-PGJ ₂ | 102 |
| 4.4.2. Kinetic parameters of PTGR1 with 15d-PGJ ₂ | 108 |
| 4.4.3. Molecular docking of 15d-PGJ ₂ into the PTGR1 active site | 110 |
| 4.4.4. Proposed catalytic mechanism | 112 |
| 5. General discussion | 117 |
| 6. Conclusions | 125 |
| 7. References | 129 |

TABLES

General Introduction

| | |
|---|----|
| Table 1: Classification of enzymes from the MDR Superfamily in eukaryotes | 24 |
| Table 2: Three-dimensional structures of AOR enzymes | 31 |

Chapter 1

| | |
|---|----|
| Table 3: Statistical parameters and solvent extraction Efficiency | 64 |
| Table 4: Methods to measure 15- <i>keto</i> -PGs | 65 |
| Table 5: Kinetic constants of human PTGR1 with α,β -unsaturated aldehydes and ketones | 68 |
| Table 6: Kinetic parameters of human PTGR1 with prostaglandins and leukotriene B ₄ | 74 |
| Table 7: Comparison of kinetic constants of mammalian PTGR1 enzymes towards prostaglandins and leukotriene B ₄ | 75 |
| Table 8: Kinetic parameters of the PTGR1 mutants | 79 |
| Table 9: IC ₅₀ values for compounds assayed as inhibitors against PTGR1 | 81 |
| Table 10: IC ₅₀ values (μM) with wild-type PTGR1 and the Arg56Ala mutant | 85 |

Chapter 2

| | |
|--|-----|
| Table 11: Kinetic parameters of wild-type and mutant PTGR1 with 15-deoxy- $\Delta^{12,14}$ -prostaglandin J ₂ | 109 |
|--|-----|

General Discussion

| | |
|--|-----|
| Table 12: Role of strictly conserved Tyr residues in Zn-independent MDRs | 120 |
|--|-----|

FIGURES

General Introduction

| | |
|--|----|
| Figure 1: Unrooted tree of Zn-independent MDRs based on the percentage of amino acid sequence identity | 26 |
| Figure 2: AOR catalytic reaction. | 27 |
| Figure 3: PTGR catalytic reaction | 27 |
| Figure 4: PTGR1 catalytic oxidation | 29 |
| Figure 5: Structures of PTGR1 substrates | 30 |
| Figure 6: Guinea-pig PTGR1 homodimer with bound NADP ⁺ and the ω -chain of 15- <i>keto</i> -PGE ₂ | 32 |
| Figure 7: Proposed catalytic mechanism for AORs | 35 |
| Figure 8: Schemes for the kinetic and catalytic mechanisms of rat PTGR1 | 36 |
| Figure 9: Diagram of the prostaglandin pathway | 38 |
| Figure 10: Formation of 15d-PGJ ₂ in the arachidonic acid cascade | 40 |
| Figure 11: Proposed catalytic mechanisms for enoyl thioester reductases | 44 |

Chapter 1

| | |
|--|----|
| Figure 12: HPLC analysis of prostaglandins and leukotriene B4 | 63 |
| Figure 13: Fluorescence quenching on NADPH and NADH binding to human PTGR1 | 67 |
| Figure 14: Determination of molecular weight by size exclusion chromatography | 69 |
| Figure 15: Protein Chip analysis of fractions after affinity chromatography of recombinant human PTGR1 | 69 |
| Figure 16: Structures of aliphatic and aromatic compounds | 71 |
| Figure 17: Structures of 15-keto-prostaglandins and leukotriene B4 used as substrates and their products | 72 |
| Figure 18: HPLC analysis of the reduction reaction of 15-keto-PGE2 by PTGR1 | 73 |
| Figure 19: Chromatogram LTB4 and 12-keto-LTB4 | 74 |
| Figure 20: Docking simulation of 15-keto-PGE2 bound into the PTGR1 active site | 77 |
| Figure 21: Alignment of PTGR1 amino acid sequences | 78 |
| Figure 22: Docking simulation of inhibitors on the active-site pocket of PTGR1 | 83 |
| Figure 23: Superimposition of indomethacin bound to the active-site pocket of guinea-pig and human PTGR1 | 84 |

Chapter 2

| | |
|--|-----|
| Figure 24: Structures of 15-keto-Prostaglandin E ₂ and 15-deoxy- Δ 12,14-Prostaglandin J ₂ used as substrates and their products | 96 |
| Figure 25: HPLC analysis of the reduction reaction of 15d-PGJ ₂ by PTGR1 | 104 |
| Figure 26: ¹ H-NMR spectrum of 15d-PGJ ₂ in the absence of enzyme | 105 |
| Figure 27: ¹ H-NMR spectrum of the reduction reaction of 15d-PGJ ₂ by PTGR1 | 106 |
| Figure 28: Expansion of a portion of the ¹ H-NMR spectrum of the products of the enzymatic reduction of 15d-PGJ ₂ corresponding to the H8 protons of the two diastereomeric products | 107 |
| Figure 29: Docking simulation of 15d-PGJ ₂ bound into the PTGR1 active site | 111 |
| Figure 30: Schematic drawing of the reaction yielding to the enolate anion intermediate in the PTGR1 reductase catalytic mechanism on two different substrates | 115 |
| Figure 31: Proposed catalytic mechanism for the reduction of 15d-PGJ ₂ by PTGR1 | 116 |

Abbreviations

| | |
|-------|--|
| AA | Arachidonic Acid |
| ADH | Alcohol Dehydrogenase |
| AOR | Alkenal/one Oxidoreductase |
| BSA | Bovine Serum Albumin |
| CAD | Cinnamyl Alcohol Dehydrogenase |
| CoA | Coenzyme A |
| COX | Cyclooxygenase |
| DMSO | Dimethylsulfoxide |
| ETR | Enoyl Thioester Reductase |
| FAS | Fatty Acid synthase |
| MDR | Medium-chain Dehydrogenase/Reductase |
| NADP | Nicotinamide Adenine Dinucleotide Phosphate |
| NADPH | Nicotinamide Adenine Dinucleotide Phosphate, reduced form |
| Nfr-2 | Nuclear factor erythroid-derived 2 |
| NF-κB | Nuclear factor κB |
| NSAID | Non-Steroidal Anti-Inflammatory Drug |
| LGA | Lamarckian Genetic Algorithms |

| | |
|----------------------|--|
| LDH | Leukotriene Dehydrogenase |
| LOX | Lipoxygenase |
| LTB ₄ | Leukotriene B ₄ |
| LTB ₄ D | Leukotriene B ₄ 12-hydroxy-dehydrogenase |
| LTB ₄ DH | Leukotriene B ₄ 12-hydroxy-dehydrogenase |
| LXA ₄ | Lipoxin A ₄ |
| PG | Prostaglandin |
| PTGR | Prostaglandin Reductase |
| PPAR _γ | Peroxisome Proliferator-Activated Receptor gamma |
| QOR | Quinone Oxidoreductase |
| SDR | Short-chain Dehydrogenase/Reductase |
| TX | Thromboxane |
| 15d-PGJ ₂ | 15-Deoxy- $\Delta^{12,14}$ -Prostaglandin J ₂ |
| 15-PGDH | 15-Hydroxyprostaglandin dehydrogenase |
| 15- <i>keto</i> -PG | 15- <i>keto</i> -Prostaglandin |

1. GENERAL INTRODUCTION

1.1. Medium-chain Dehydrogenases/Reductases

Our knowledge on the superfamily of medium-chain dehydrogenases/reductases (MDRs) has grown considerably in recent years, and it currently includes over 15,000 members and 500 families¹. Some families are alcohol dehydrogenases (ADHs), quinone oxidoreductases (QORs), and alkenal/one oxidoreductases (AORs). Basically we can divide the MDRs into two groups: one of them, Zn-dependent MDRs (with two Zn atoms per subunit, one catalytic and one structural), mainly use NAD(H) as a cofactor; the second one, Zn-independent MDRs, often use NADP(H) as a cofactor¹ (Table 1).

MDR proteins share a three-dimensional structure, with subunits of approximately 350 residues, generally combining into homodimers (although some members are active as monomers or tetramers). Each subunit contains two domains: a catalytic domain that comprises both the amino and carboxyl terminal ends of the protein, and a cofactor-binding domain, with the classical Rossmann fold². The two domains are separated by a cleft containing a deep pocket which accommodates the active site.

In eukaryotes the MDR superfamily can be divided into separate families, based on the amino acid sequence identity³. The largest MDR families are currently Alcohol Dehydrogenase (ADH), Cinnamyl Alcohol Dehydrogenase (CAD) and Alkenal/one Oxidoreductase (AOR) families, although the functional importance of each family is not correlated with their size.

Table 1. Classification of enzymes from the MDR superfamily in eukaryotes

| | | FAMILY |
|-----------------------|------------------------|---|
| Zn-Dependent | MACROFAMILY I | Polyol Dehydrogenase (PDH) |
| | | Alcohol Dehydrogenase (ADH) |
| | MACROFAMILY II | Yeast Alcohol Dehydrogenase (Y-ADH) |
| | | Cinnamyl Alcohol Dehydrogenase (CAD) |
| Zn-Independent | MACROFAMILY III | Alkenal/one Oxidoreductase (AOR) |
| | | Enoyl Thioester Reductase (ETR) |
| | | Nuclear Receptor Binding Protein (NRBP) |
| | | Quinone Oxidoreductase (QOR) |

Data taken from Riveros-Rosas *et al.*⁴ and Persson *et al.*³

1.2. Zn-independent MDRs

Zn-independent MDRs include a very heterogeneous group of proteins, which has been scarcely described until now. This group shows enzymatic activities and biological functions quite different from that of the Zn-dependent MDRs (i.e., the well-known reversible oxidation of alcohols to aldehydes, prototypical of ADHs). In fact, the former group offers some features not always related to enzymatic activity, such as that of the Nogo-interacting mitochondrial protein, which is a potent inhibitor of regeneration following spinal cord injury⁵, or as transcription factors like the nuclear receptor binding protein (NRBP)⁶ or as a DNA-binding factor⁷, which later turned out to be a *trans*-2-enoyl thioester reductase⁸.

As for the enzymatic activities, Zn-independent MDRs are catalyzing the following reactions: reduction of the double bond at α,β position with respect to a carbonyl group⁹, irreversible leukotriene B₄ oxidation¹⁰, reduction of quinones¹¹, reduction of azo carbonyl imides¹² and double-bond reduction of fatty acid nitroalkenes¹³, among others. The α,β unsaturation may be that of alkenals or alkenones¹⁴, in AORs, and also that of enoyl thioesters attached to CoA¹⁵ or the acyl carrier protein group¹⁶, in ETRs. The vast majority of Zn-independent MDRs described thus far are NADP(H) dependent, and thus reduction reactions are favored given the high intracellular [NADPH]:[NADP⁺] ratio.

Figure 1 shows a phylogenetic tree featuring Zn-independent MDRs, where three major families are highlighted: AORs, ETRs and QORs.

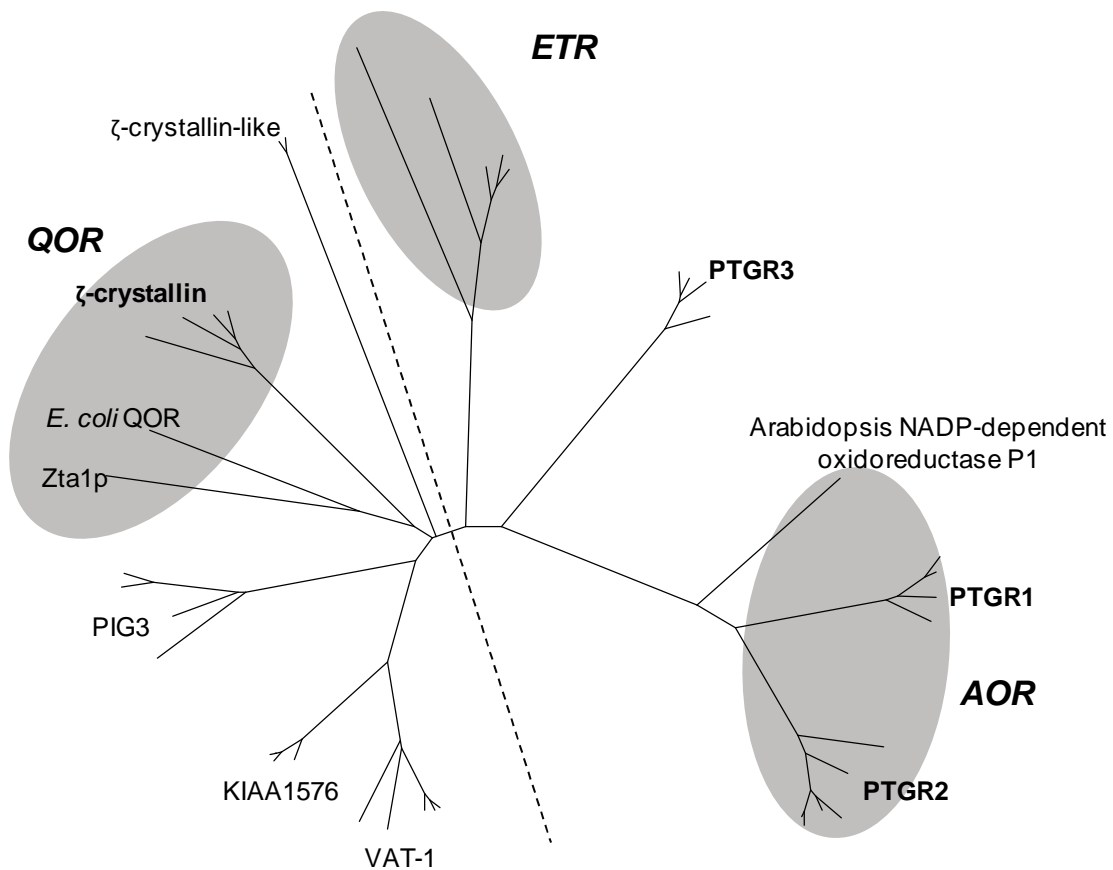


Figure 1: Unrooted tree of Zn-independent MDRs based on the percentage of amino acid sequence identity. Sequences included only vertebrate proteins, except for ETR from *Candida* sp., Arabidopsis NADP-dependent oxidoreductase P1, Zta1p from *Saccharomyces cerevisiae* and QOR from *E. coli*. Protein subfamilies considered are ζ -crystallin, ζ -crystallin-like, PIG3 (p53-inducible gene 3), KIAA1576, VAT-1, PTGR1, PTGR2 and PTGR3. Shaded ovals indicate clusters including three major protein families: alkenal/one oxidoreductase (AOR), enoyl thioester reductase (ETR) and quinone oxidoreductase (QOR). Dashed line separates the QOR from ETR and AOR families. Adapted from Ref ¹⁷.

1.3. Alkenal/one oxidoreductases

The most characteristic enzymatic activity of AORs is the NADPH-dependent hydrogenation of the double bond of α,β -unsaturated alkenals and alkenones. (Fig. 2).

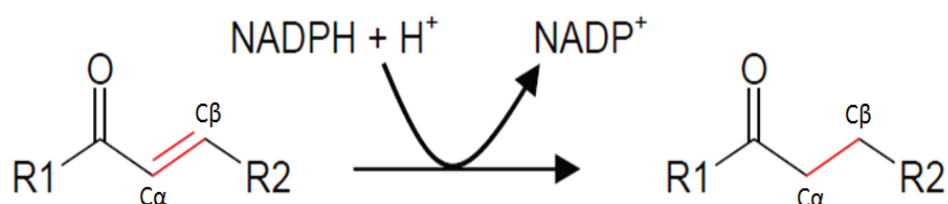


Figure 2: AOR catalytic reaction. Reduction of the double bond at position α,β to the carbonyl group. Reproduced from Ref ¹⁸.

The AOR family includes Arabidopsis NADP-dependent oxidoreductase P1 and three human prostaglandin reductases (PTGRs), PTGR1¹⁹, PTGR2 (or ZADH1)²⁰ and PTGR3 (or ZADH2)²¹, sharing only 12% amino acid sequence identity, while PTGR1 and PTGR2 are the most closely related with 37% identity. The three PTGRs are able to reduce 15-*keto*-PGs to inactive 13,14-dihydro-15-*keto*-PGs (Fig. 3), with different tissue specificity²¹.

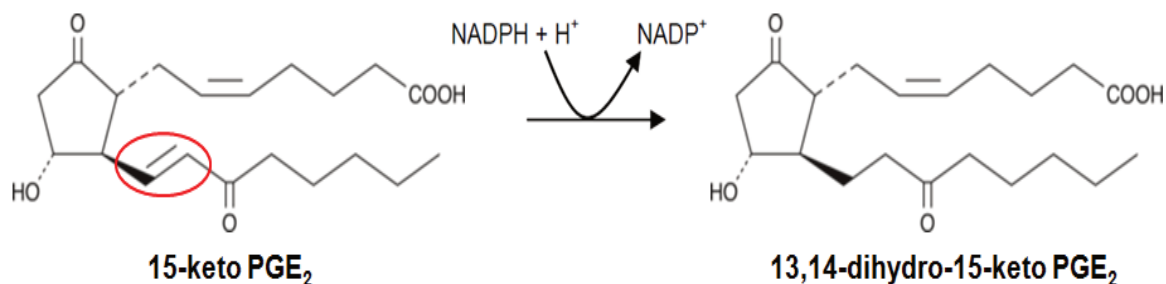


Figure 3: PTGR catalytic reaction. Reduction of the double bond at position α,β to the carbonyl group of a 15-*keto*-PGs (illustrated with 15-*keto*-PGE₂). Reproduced from Ref ¹⁸.

1.4. Prostaglandin reductase 1 (PTGR1)

PTGR1 was the first enzyme described in this family. The multifunctional PTGR1 is a key enzyme in the irreversible degradation of various eicosanoids, such as prostaglandins¹⁹, leukotrienes²², and lipoxins²³. All these compounds are endogenous lipid mediators, crucial in a wide range of normal physiological and pathological processes, such as inflammation or defense responses.

PTGR1 has received different names over time, such as prostaglandin reductase (PTGR or PGR) or leukotriene dehydrogenase (LTD), owing to its various reactions catalyzed. The reduction of the 13,14 double bond of 15-*keto*-PGs has been described in different species such as human^{24,25}, chicken²⁶, pig⁹, guinea pig²⁷ and rat¹⁴. Actually, the PTGR1 activity from human placenta was described in the mid-70s. In the early 90s, Yokomizo *et al.* purified an enzyme from porcine kidney that was capable of carrying out the oxidation of a hydroxyl group of leukotriene B₄ (LTB₄)^{10,28}, and thus they named the enzyme as leukotriene B₄ 12-hydroxy-dehydrogenase (LTB₄DH, LTB₄D) (Fig. 4). In the late 90s, Ensor *et al.* purified PTGR1 from porcine lung and, surprisingly, the primary structure of PTGR1 was identical to that of LTB₄DH, indicating that the enzyme is capable of carrying out the reduction of a double bond as well as the oxidation of a hydroxyl group⁹. However, the specific activity of PTGR1 with 15-*keto*-PGs as a substrate is much higher than that of the oxidation of LTB₄.

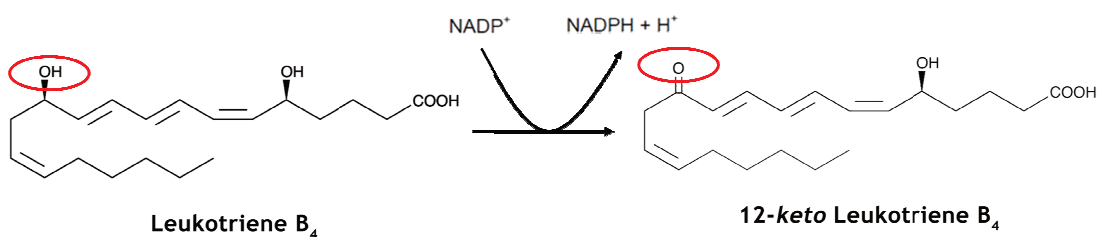


Figure 4: PTGR1 catalytic oxidation. Oxidation of a hydroxyl group of LTB₄.

Later, yet another reaction was also observed towards 15-*keto*-LXA₄, generating 13,14-dihydro-LXA₄²³. It appears to be very similar to the reduction of the 13,14 double bond of 15-*keto*-PGs. The last activity that has been verified is the double bond reduction of fatty acid nitroalkenes¹³. A wide kinetic study was performed in rat PTGR1 with various α,β -unsaturated aldehydes and ketones, which suggested a potent antioxidative activity of this enzyme, acting to protect against reactive oxygen species¹⁴.

In summary, the multifunctional PTGR1 is a key enzyme in the irreversible degradation of eicosanoids (PGs, LXA₄ and LTB₄), fatty acid nitroalkenes and α,β -unsaturated aldehyde/ketones (Fig. 5).

Since then the enzyme has been studied from different scientific viewpoints. The most complete immunohistochemical analysis was performed in guinea-pig, where the enzyme was found in liver, kidney, small intestine, spleen and stomach²⁷. In human tissues, the enzyme is mostly expressed in kidney and liver²⁸.

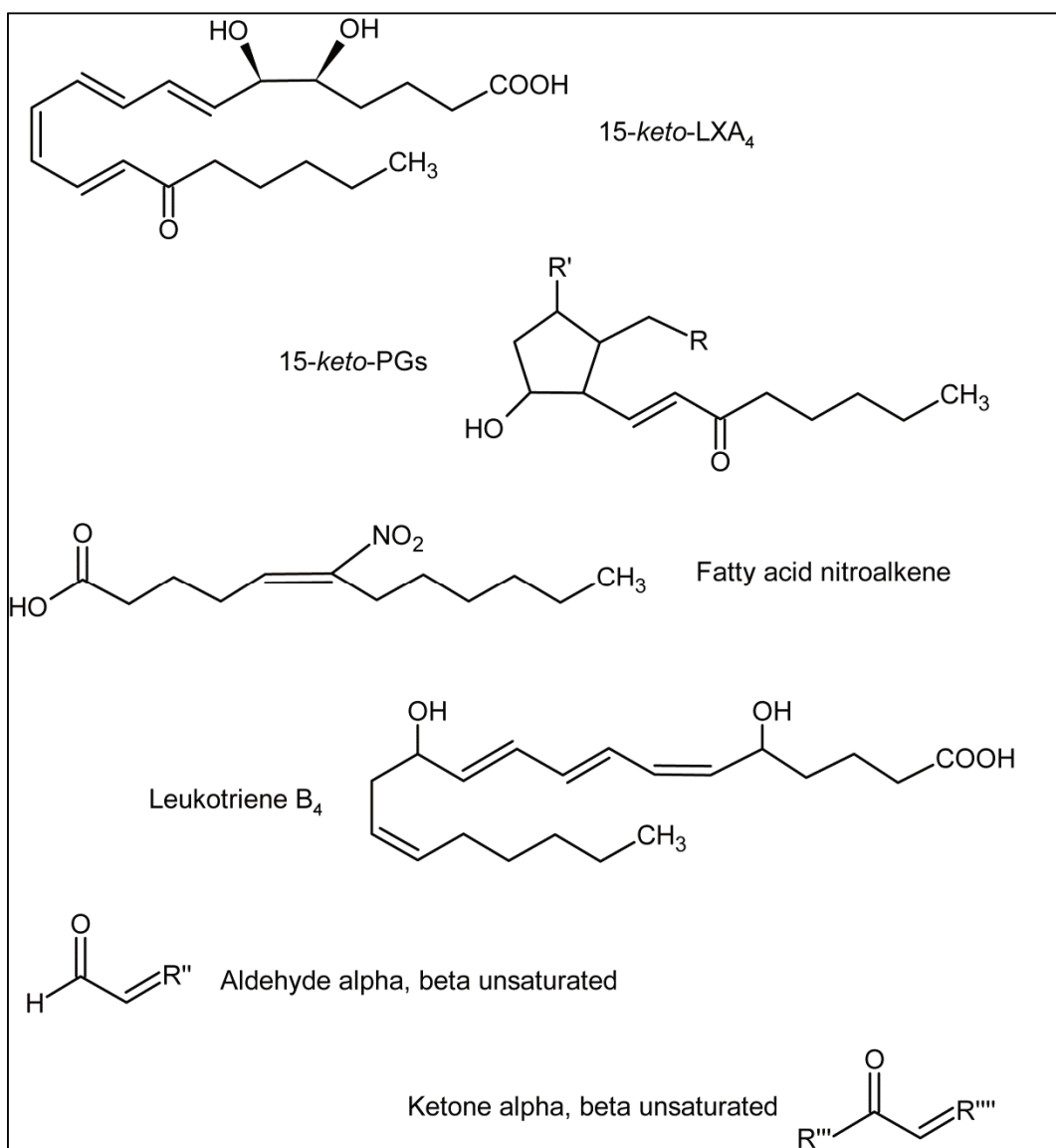


Figure 5: Structures of PTGR1 substrates. Eicosanoids (15-*keto*-PGs, 15-*keto*-LXA₄ and LTB₄), fatty acid nitroalkenes and α,β -unsaturated aldehydes/ketones.

The three-dimensional structure of PTGR1 has been solved by X-ray crystallography for the human and guinea-pig^{29,30} enzymes (Table 2). Especially relevant are the ternary complexes of guinea-pig PTGR1 with NADP⁺ and 15-*keto*-PGE₂ (Fig. 6) and with NADP⁺ and indomethacin. PTGR1 appears to be a dimer in the asymmetric unit, with the exception of the complex with raloxifene which is a monomer.

Table 2. Three-dimensional structures of AOR enzymes

| Enzyme | Species | Cofactor | Ligand | Resolution (Å) | PDB code | Release |
|--------|--------------------|-------------------|-----------------------------------|----------------|----------|----------|
| PTGR1 | guinea pig | NADP ⁺ | – | 2.30 | 1V3T | Jul 2004 |
| | guinea pig | – | – | 2.00 | 1V3U | Jul 2004 |
| | guinea pig | NADP ⁺ | 15- <i>keto</i> -PGE ₂ | 2.00 | 1V3V | Jul 2004 |
| | human | – | – | 2.30 | 1ZSV | Jun 2005 |
| | guinea pig | NADP ⁺ | indomethacin | 2.00 | 2DM6 | Nov 2006 |
| | human | NADP ⁺ | raloxifene | 2.20 | 2Y05 | Jan 2011 |
| PTGR2 | mouse | – | – | 2.10 | 1VJ1 | Dec 2003 |
| | human | NADPH | – | 2.00 | 2ZB3 | Sep 2008 |
| | human | NADP ⁺ | 15- <i>keto</i> -PGE ₂ | 1.63 | 2ZB4 | Sep 2008 |
| | human | NADPH | nicotinamide | 1.80 | 2ZB7 | Sep 2008 |
| | human | NADP ⁺ | indomethacin | 2.00 | 2ZB8 | Sep 2008 |
| | human | NADP ⁺ | glycyrrhetic acid | 2.00 | 2W4Q | Jan 2009 |
| | human | NADP ⁺ | – | 2.17 | 2VNA | Feb 2009 |
| | human | NADP ⁺ | phenylbutazone | 1.85 | 2W98 | Abr 2009 |
| PTGR3 | human | NADP ⁺ | – | 1.45 | 2C0C | Sep 2005 |
| | human | NADP ⁺ | diclofenac | 1.90 | 2WEK | Dec 2009 |
| | human | NADP ⁺ | raloxifene | 1.75 | 2X1H | Nov 2010 |
| | human | NADP ⁺ | fenoprofen | 1.60 | 2X7H | Dec 2010 |
| AOR | <i>A. thaliana</i> | – | – | 2.50 | 2J3H | Oct 2006 |
| | <i>A. thaliana</i> | NADP ⁺ | – | 2.80 | 2J3I | Oct 2006 |
| | <i>A. thaliana</i> | NADP ⁺ | <i>p</i> -coumaric acid | 2.80 | 2J3J | Oct 2006 |
| | <i>A. thaliana</i> | NADP ⁺ | 4-hydroxynonenal | 2.80 | 2J3K | Oct 2006 |

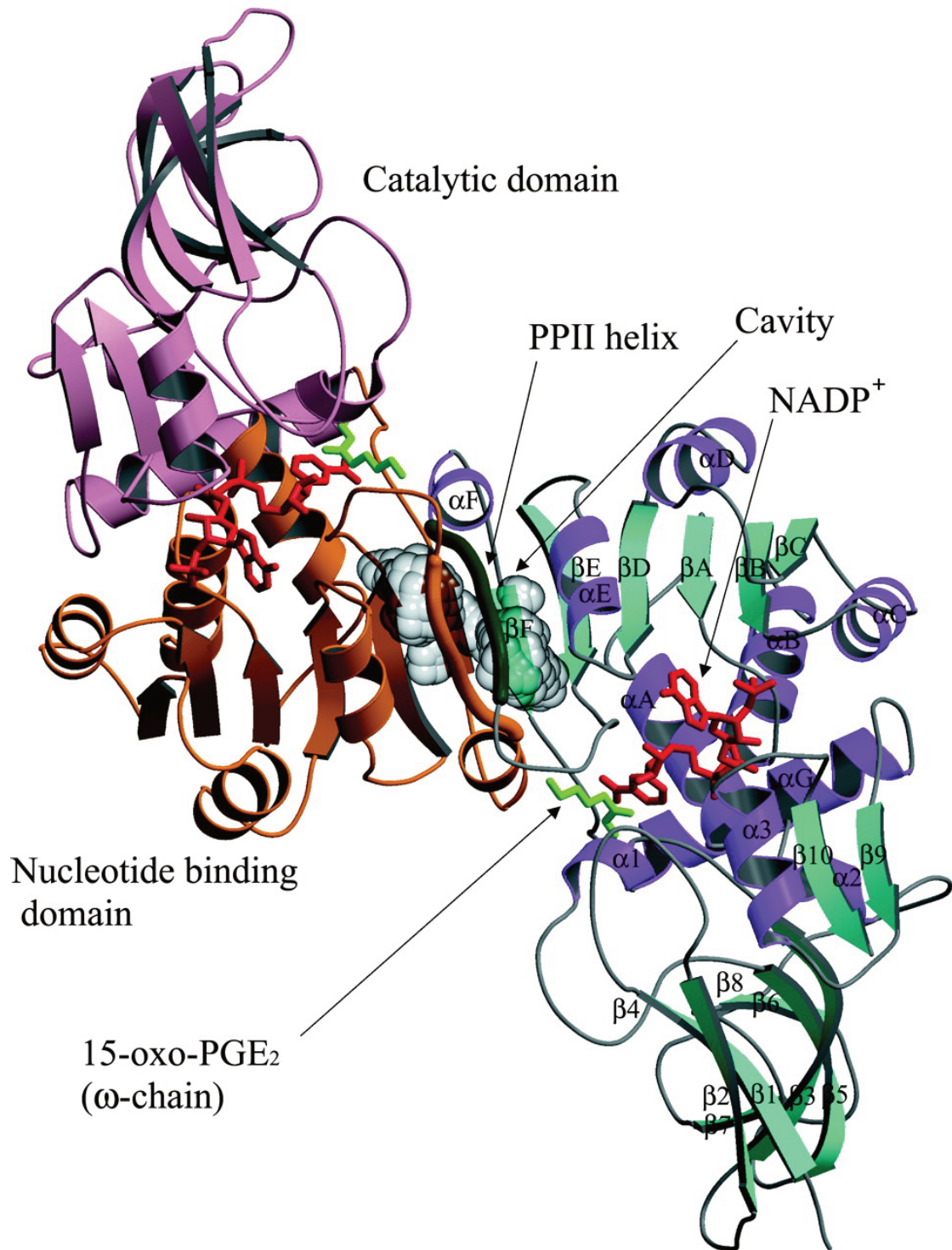


Figure 6: Guinea-pig PTGR1 homodimer with bound NADP⁺ and the ω -chain of 15-keto-PGE₂. The catalytic and nucleotide-binding domains are colored *pink* and *orange* in the upper subunit, and α -helices, β -strands, and left-handed polyproline helix type II (PPII helix) are shown in *cyan*, *magenta*, and *deep green*, respectively in the bottom subunit. NADP⁺ is in *red*, and the ω -chain of 15-keto-PGE₂ is in *green*. PPII at the dimer interface is emphasized as *bold coil*. The intersubunit cavity is shown in *gray* CPK. PDB code 1V3V. Reproduced from Ref ²⁹.

1.5. Prostaglandin reductases 2 and 3

Human PTGR2 (also known as zinc-binding alcohol dehydrogenase domain-containing 1, ZADH1) is the second best known enzyme from the AOR family. The three-dimensional structures of human and mouse PTGR2 have been solved (Table 2). Unlike other MDR proteins, PTGR2 appears to be a monomer in the asymmetric unit and this has been confirmed by size exclusion chromatography (J. Mesa, unpublished data). Similarly to PTGR1, PTGR2 is able to perform the reduction of the 13,14 double bond of 15-*keto*-PGs, although it cannot oxidize the hydroxyl group of LTB₄. PTGR2 is present in several tissues, i.e. kidney, liver, pancreas, prostate and heart³¹. PTGR2 is up-regulated in the late phase of adipocyte differentiation and predominantly distributed in adipose tissue³². Ectopic overexpression of PTGR2 in T3T3-L1 cells dramatically inhibits adipocyte differentiation (repressing the transcriptional activity of PPAR γ)³². Some studies hypothesized that PTGR2 may play a role in gastric³³ and pancreatic³⁴ cancers.

Human PTGR3 (also known as zinc-binding alcohol dehydrogenase domain-containing 2, ZADH2) is a peroxisomal enzyme (E. Yakovtseva, unpublished data). Several *holo*-PTGR3 3D structures have been deposited (Table 2), in complex with common prescription drugs (fenoprofen, raloxifene and diclofenac). PTGR3 appears to be a monomer in the asymmetric unit. *Yu et al.*²¹ showed that PTGR3 is a negative regulator of adipocyte differentiation. PTGR3 is downregulated in the early stage of the adipogenesis process²¹. The enzymatic activity in front of 15d-PGJ₂ (a

potent endogenous ligand for PPAR γ) indicates that PTGR3 may play a role in adipocyte differentiation²¹.

1.6. Catalytic and kinetic mechanisms of PTGRs

The available 3D structures of PTGRs, along with those of Arabidopsis AOR (Table 2), also including ternary complexes, has allowed proposing a catalytic mechanism for the α,β -double bond hydrogenation of alkenals, alkenones and 15-*keto*-prostaglandins (Fig. 7). The formation of an enolate anion is proposed as a transition-state intermediate, which would be stabilized by a side-chain hydroxyl group^{16,29,35}. This hydroxyl group is contributed by a strictly conserved Tyr residue (Tyr245 in guinea-pig PTGR1²⁹ and Tyr 260 in Arabidopsis AOR¹⁶), although in PTGR1 the 2'-hydroxyl group of the NADPH ribose may participate more directly. Site-directed mutagenesis studies on this Tyr245³⁶ or the homologous Tyr of PTGR2^{20,32} show that this residue participates in catalysis, although it does not play an essential role because the mutant enzyme preserved part of its activity (Fig. 7).

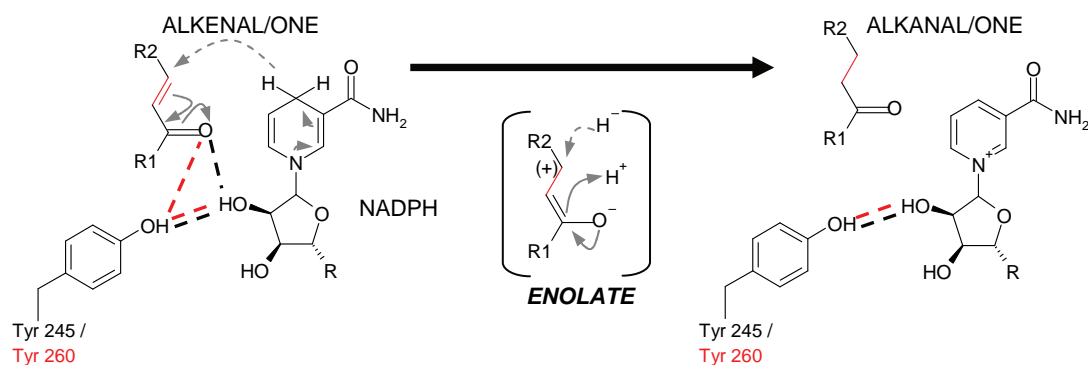


Figure 7: Proposed catalytic mechanism for AORs. Hydride electrons perform the nucleophilic attack on the C β , where electron density is ultimately shifted to the carbonyl oxygen leading to the formation of an enolate intermediate. This intermediate may capture a proton to yield the reduced product. The hydrogen bonds are indicated with dashed lines, while the nucleophilic attack is indicated with arrows. The nucleophilic attack of the hydride from nicotinamide ring is indicated by dashed arrows. The hydrogen bonds in black are described in the ternary complex of guinea-pig PTGR1 (having Tyr245) with 15-*keto*-PGE₂, while the red hydrogen bonds are described in the ternary complexes of Arabidopsis AOR (having Tyr260) with 4-hydroxynonenal and *p*-coumaric acid. R1: C_n or H, R2: C_n. Reproduced from Ref ³⁷.

The kinetic mechanism of rat PTGR1 using 3-nonen-2-one was also elucidated and it was found to conform a Theorell-Chance kinetic mechanism, with NADPH binding first and NADP⁺ leaving last³⁸, similar to that previously described for ADHs (Fig. 8A). First, the cofactor (NADPH) binds, causing a conformational change which allows substrate binding. Next, rapid catalysis and dissociation of the product occurs, followed by a slower dissociation of the cofactor (NADP⁺). Note that the reduction of the α,β -double bond is hardly reversible. Similarly to other MDR enzymes, PTGR1 catalyzes the hydride transfer in a regio- and stereospecific manner, as it promotes the transfer of the pro-*R* hydride from NADPH to the β -carbon of an α,β -unsaturated ketone (Fig. 8B).

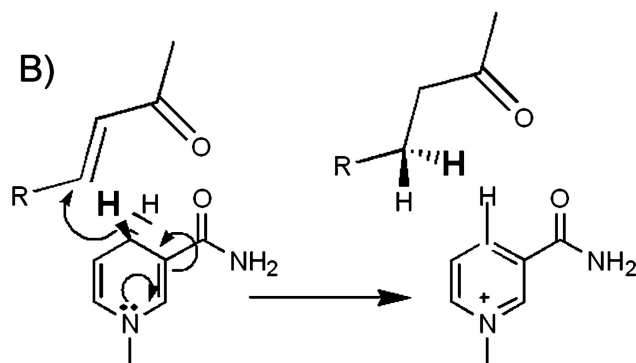
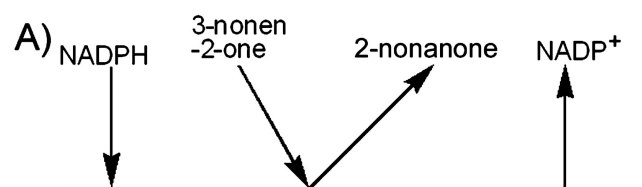


Figure 8: Schemes for the kinetic and catalytic mechanisms of rat PTGR1. *A*, Reduction of 3-nonen-2-one by rat PTGR1 has been found to conform to an ordered Theorell-Chance kinetic mechanism (a special case of a sequential ordered Bi Bi mechanism where the steady-state concentrations of the ternary complexes are kinetically negligible) with NADPH binding first and NADP⁺ leaving last. *B*, Rat PTGR1 was found to catalyze the transfer of the pro-*R* hydride of NADPH to what becomes the *R*-position hydrogen of the β -carbon. Reproduced from Ref ³⁸.

1.7. Physiological role of PTGRs

1.7.1. Prostaglandins (PGs)

PGs are endogenous substrates of PTGRs. They are lipid compounds derived from arachidonic acid (AA) by the action of cyclooxygenases, acting locally as messenger molecules by binding to different types of receptors in a wide variety of physiological processes, such as smooth muscle contraction and relaxation, blood vessel dilation and constriction adipocyte differentiation, and modulation of inflammation. PG metabolism begins with the release of AA from membrane phospholipids by phospholipase A₂, then brought to either the cyclooxygenase pathway to form prostaglandins and thromboxanes or to the lipoxygenase pathway to yield leukotrienes³⁹ (Fig. 9).

All these metabolites must be degraded rapidly once they have performed their functions. For this reason, there is a defined mechanism of catalysis which inactivates these compounds by the initial oxidation of their 15(*S*)-hydroxyl group catalyzed by NAD⁺-linked 15-hydroxyprostaglandin dehydrogenase (15-PGDH)⁴⁰. Next, PTGRs catalyze the conversion of 15-*keto*-PGs to the fully inactive 13,14-dihydro-15-*keto*-PGs by hydrogenation of the 13,14 double bond.

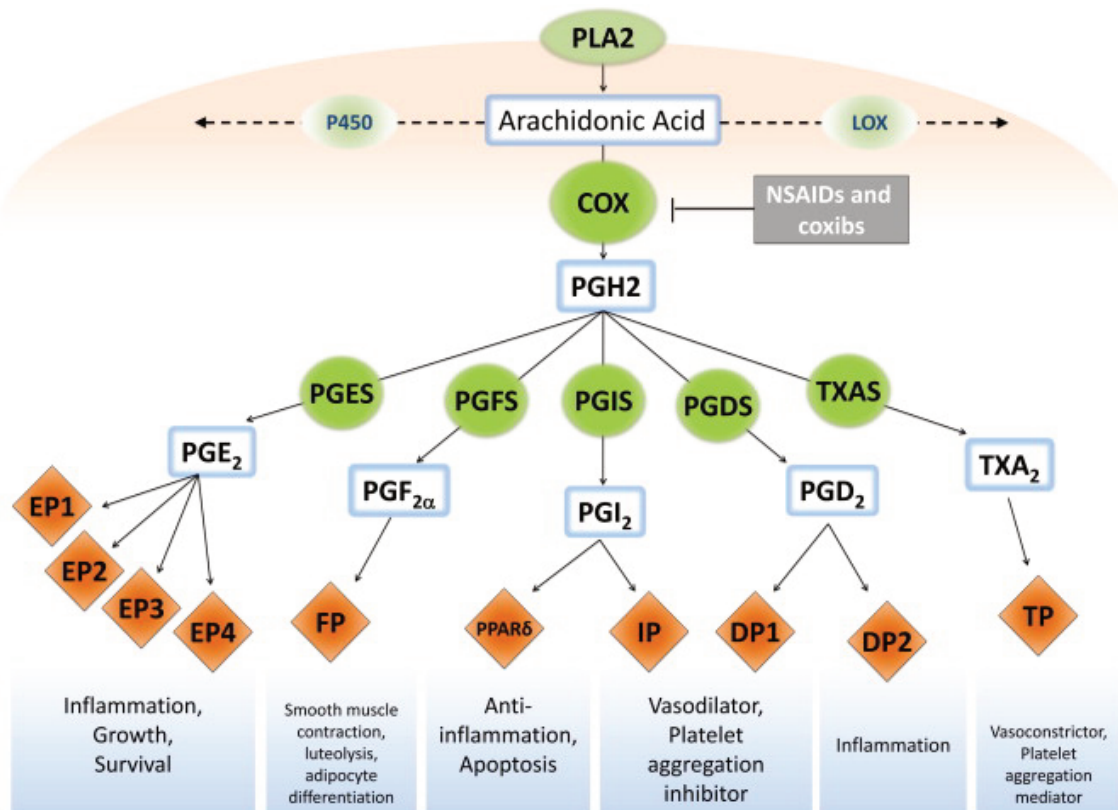


Figure 9: Diagram of the prostaglandin pathway. Arachidonic acid is a polyunsaturated fatty acid that constitutes the phospholipid domain of most cell membranes and is liberated from the cellular membranes by cytoplasmic phospholipase A₂. Free arachidonic acid can be metabolized to eicosanoids through three major pathways: the cyclooxygenase (COX), the lipoxygenase (LOX) and the cytochrome P450 monooxygenase pathways. In the COX pathway, the key step is the enzymatic conversion of arachidonic acid to the intermediate PGG₂, which is then reduced to PGH₂ by the peroxidase activity of COX. PGH₂ is sequentially metabolized to prostanoids, including prostaglandins (PGs) and thromboxanes (TXs) by specific prostaglandin and thromboxane synthases. Each of the PGs exerts its biological effects by binding to its cognate G protein-coupled receptor. Reproduced from Ref³⁹.

15-Deoxy- $\Delta^{12,14}$ -Prostaglandin J₂ (15d-PGJ₂) is a highly reactive electrophilic molecule, an important redox signaling mediator and a natural ligand of peroxisome proliferator-activated receptor gamma (PPAR γ), a member of the nuclear receptor superfamily and a ligand-activated transcription factor with pleiotropic effects on adipocyte differentiation, glucose homeostasis, lipid metabolism, growth, and inflammation. To activate PPAR γ , a ligand is needed for binding to its ligand-binding domain. However, some effects of 15d-PGJ₂ are mediated through receptor-independent pathways.

Like other PGs, 15d-PGJ₂ is derived from PGH₂, which is converted by PGD synthase to PGD₂ and further chemically dehydrated to form 15d-PGJ₂⁴¹ (Fig. 10). Furthermore, 15d-PGJ₂ is also involved in the resolution of inflammatory responses⁴¹. The molecule contains two electrophilic carbons at positions 9 and 13, which exert distinct contributions to the biological activity of 15d-PGJ₂. Inactivation of 15d-PGJ₂ can be achieved by double-bond hydrogenation catalyzed by PTGRs.

Several prostaglandins act as bioactive modulators for regulating adipocyte differentiation through either direct binding on the PPAR γ ligand-binding domain or indirect mechanisms mediated by signaling transduction. Modulation of PTGRs expression or activity might provide a novel avenue in treating obesity and related metabolic disorders.

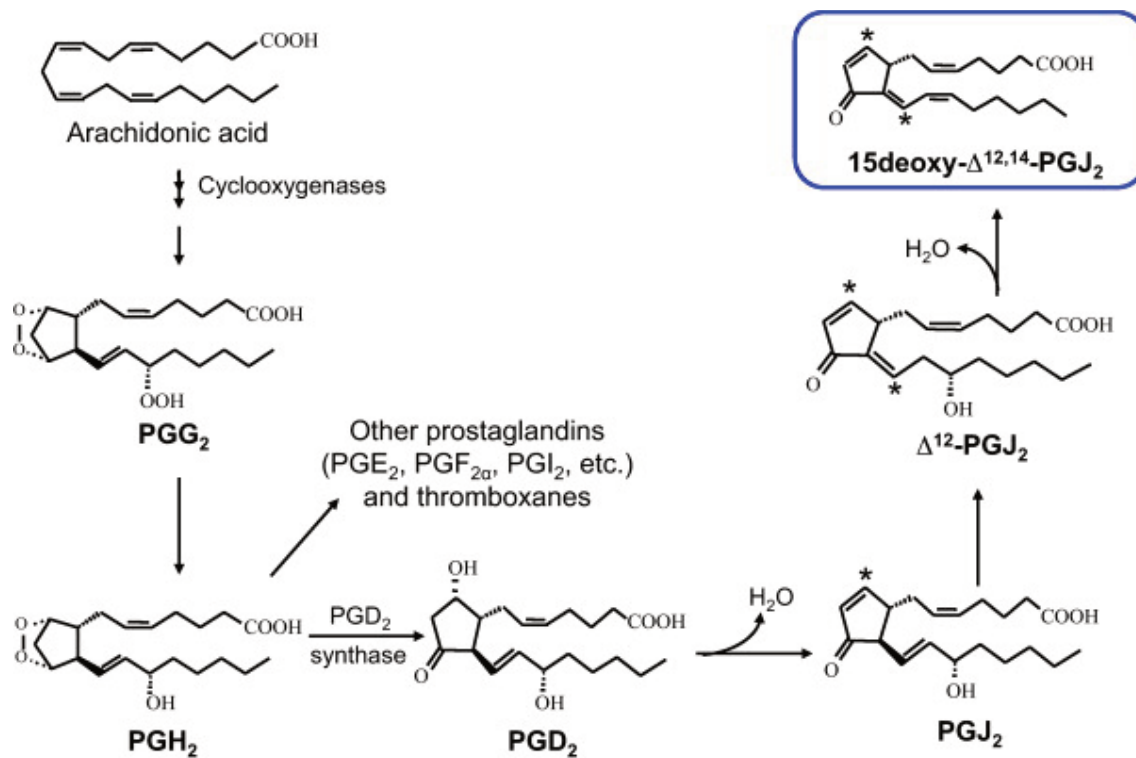


Figure 10: Formation of 15d-PGJ₂ in the arachidonic acid cascade. 15d-PGJ₂ and its precursors cyclopentenone prostaglandins have electrophilic carbon(s), designated with asterisks, due to the α,β-unsaturated carbonyl group. Reproduced from Ref ⁴¹.

1.7.2. PTGRs and cancer

Several reports have linked PTGR1 and cancer, although with opposing effects on cell proliferation. Thus, PTGR1 upregulation was found associated with several cancer types, such as hepatocarcinoma⁴², bladder⁴³ and prostate cancer⁴⁴ and thus it could be considered a potential biomarker. Likewise, PTGR1 knockdown suppressed proliferation and colony formation ability, and induced cell cycle arrest in gastric and prostate cancer cells⁴⁵.

In contrast, PTGR1 restoration of the enzyme expression in PTGR1-negative (H1299) or PTGR1-low (A549) lung cancer cell lines induced apoptosis and growth inhibition *in vitro*. Ectopic expression of PTGR1 also caused the suppression of tumorigenicity of A549 cells in an athymic nude mice model⁴⁶. In this regard, naturally occurring compounds, such as gallic acid and calycosin, suppressed the *in vitro* oncogenic transformation of HepG2 cells via the induction of PTGR1 expression^{47,48}, and curcumin and resveratrol enhanced cytotoxicity of hydroxymethylacylfulvene against HepG2 and SW620 cells through PTGR1 upregulation⁴⁹. PTGR1 was also found to be induced in rats⁵⁰ and in various human colon cancer cell lines and HepG2 cells by 1,2-dithiole-3-thione⁵¹ (a synthetic analog of compounds with chemopreventive activity isolated from cruciferous vegetables). In the former rat study, the authors hypothesized that PTGR1 could act by suppressing inflammatory processes related to carcinogenesis⁵⁰. In the latter human studies, PTGR induction sensitized tumor cells to anticancer agents by increasing their cytotoxicity⁵¹. In addition, PTGR1 participates in the activation of some prodrugs used in antitumor chemotherapy (i.e. CS-670⁵² and hydroxymethylacylfulvene^{49,53}).

Given the implication of PTGRs in several cancer types, searching inhibitor compounds against PTGRs becomes pharmacologically relevant. Three NSAIDs (diclofenac, indomethacin and niflumic acid) were tested against porcine PTGR1, displaying high inhibitory potency *in vitro*⁵⁴. As mentioned above, several drugs approved for therapy bind to PTGRs, as demonstrated by their corresponding ternary complexes: diclofenac to human PTGR3, indomethacin to guinea-pig PTGR1 and human PTGR2, fenoprofen to human PTGR3, phenylbutazone (only for veterinary use) to human PTGR2, raloxifene (an estrogen receptor modulator used in treatment and prevention of osteoporosis and invasive breast cancer in postmenopausal women) to human PTGR1 and PTGR3. Thus the interaction of these compounds with PTGRs merits further investigation as it may explain some of their pharmacological effects and disclose novel uses through drug repositioning.

1.8. Enoyl thioester reductases

ETRs catalyze the α,β -double bond reduction of *trans*-2-enoyl thioesters (Fig. 11). Most ETRs are enzymes from the short-chain dehydrogenase/reductase (SDR) superfamily¹⁶, but the ETR domain of fatty acid synthase type I (FAS I)⁵⁵ and mitochondrial *trans*-2-enoyl-CoA reductase (MECR)^{15,56} belong to the MDR superfamily, conforming two different families of MDR, FAS and MECR, respectively³. The reduction reaction of enoyl thioesters is the last step in the pathway for the *de novo* synthesis of lipids. This pathway includes a sequence of reactions which is identical in all organisms, catalyzed by a multienzyme complex called fatty acid synthase (FAS). Its structure and subcellular localization are different between species. While mitochondria from bacteria, plants, protozoa and apicomplexes use a series of monofunctional enzymes, called fatty acid synthase type II (FAS II)⁵⁷, vertebrates have a single multifunctional protein of 274 kDa. This protein, called FAS I and active as a dimer, presents different domains that catalyze all the reactions in this pathway.⁵⁵

The 3D structures of human¹⁵ and *Candida*⁵⁶ MECRs and porcine FAS I⁵⁵ have been solved. In the case of MECR, the cofactor-binding domain presents an additional β -sheet between the fifth β -sheet and fifth α -helix. As for the catalytic mechanism of ETRs, the reaction is very similar to that of AORs, as it requires in α,β -double bond hydrogenation and therefore an enolate intermediate and a proton donor. Again this proton could be contributed by a Tyr residue (Tyr94 in human MECR, which is highly conserved), and site-directed mutagenesis studies have been shown this residue to act as a catalytic residue¹⁵. Recently a new mechanism has been

proposed by Rosenthal *et al.*⁵⁸, for crotonyl-CoA carboxylase/reductase (a bacterial MDR enzyme), where a covalent ene adduct intermediate is formed between cofactor and substrate. The classical mechanism for ETRs assumed a direct hydride transfer from NADPH onto the substrate to create an enolate intermediate, which was subsequently protonated to yield the reaction products. The ene mechanism would proceed through a distinct C2-ene intermediate which would be subsequently protonated (Fig. 11). Some evidence has also been reported for an adduct of NADPH with the enoyl thioester substrate on the reaction catalyzed by enoyl-acyl carrier protein reductase from cyanobacteria⁵⁹.

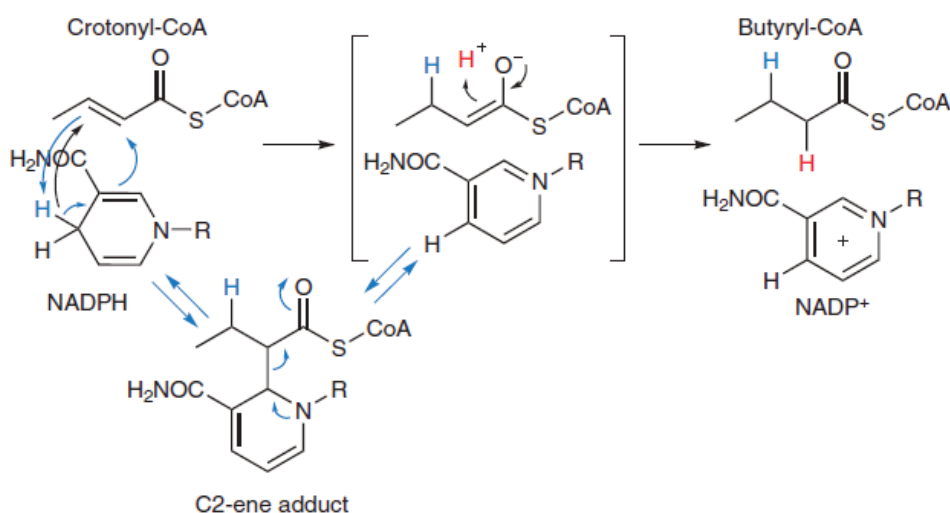


Figure 11: Proposed catalytic mechanisms for enoyl thioester reductases. Classical mechanism (black arrows) assumes a direct hydride transfer from NADPH onto the substrate to create an enolate intermediate. Ene mechanism (blue arrows) proceeds through a distinct C2-ene intermediate (in brackets) and subsequently protonated. Reproduced from Ref ⁵⁸.

The following sections of this Thesis dissertation are presented as independent chapters, each one including its own introduction and discussion, since they are intended to be the basis for further publications.

2. OBJECTIVES

2. Objectives

The enzymatic properties of PTGR1 have been partially investigated in other species, such as pig, guinea pig and rat. However, only few reports on human PTGR1 existed in the literature, one of them with the enzyme isolated from placental tissue and using NADH as a cofactor. As for the accurate determination of the kinetic constants with PGs, one serious drawback was the lack of an analytical method sensitive enough to detect submicromolar concentrations of substrate. Finally, a previous study on the reduction of 15d-PGJ₂ catalyzed by rat PTGR1 did not provide the unambiguous identification of the reaction product nor the catalytic mechanism. Therefore, a complete characterization of the reaction of human PTGR1 with 15d-PGJ₂ was lacking.

The main goals of this work have been to develop a new method of analysis of PGs, to complete the enzymatic characterization of human PTGR1, using also molecular docking simulations, site-directed mutagenesis studies and the inhibition analysis, and the elucidation of the catalytic mechanism with 15d-PGJ₂.

Partial objectives:

1. To develop an HPLC-based assay for an accurate measure of 15-*keto*-PGs activity at submicromolar concentrations of substrate.
2. To perform an extensive kinetic characterization of PTGR1 in front aldehydes, ketones and 15-*keto*-PGs.

3. To analyze the PTGR1 structure (PDB ID 2Y05), characterizing its quaternary structure and the substrate binding center.
4. To perform a site-directed mutagenesis study to define the most important residues in the catalytic mechanism in human PTGR1.
5. To carry out an inhibition analysis using non-steroidal anti-inflammatory drugs (NSAIDs) as potential inhibitors.
6. To perform the kinetic characterization of human PTGR1 in front of 15d-PGJ₂.
7. To carry out a site-directed mutagenesis to pinpoint essential amino acid residues in the catalysis of human PTGR1 with 15d-PGJ₂.
8. To identify the products of human PTGR1 activity on 15d-PGJ₂, using ¹H and ¹³C NMR spectroscopy.
9. To propose a catalytic mechanism for the α,β double-bond hydrogenation of 15d-PGJ₂ by human PTGR1.

3. CHAPTER 1

Human prostaglandin reductase 1 (PTGR1): Substrate specificity, inhibitor analysis and site- directed mutagenesis

Some of the results of this chapter appear in the publications:

Mesa J, Alsina C, Oppermann U, Parés X, Farrés J, Porté S. **Human prostaglandin reductase 1 (PTGR1): Substrate specificity, inhibitor analysis and site-directed mutagenesis.** *Chem. Biol. Interact.* **234**, (2015) 105–113.

Mesa J, Farrés J, Porté S, Parés X. **A new HPLC-based method for the determination of the 15-ketoprostaglandin reductase activity.** Abstrat resented at the XXXVI Congreso de la SEBBM, Madrid 2013.

3.1. Abstract

Prostaglandins (PGs) are lipid compounds derived from arachidonic acid by the action of cyclooxygenases, acting locally as messenger molecules in a wide variety of physiological processes, such as inflammation, cell survival, apoptosis, smooth muscle contraction, adipocyte differentiation, vasodilation and platelet aggregation inhibition. In the inactivating pathway of PGs, the first metabolic intermediates are 15-*keto*-PGs, which are further converted into 13,14-dihydro-15-*keto*-PGs by different enzymes having 15-*keto*-PG reductase activity. Three human PG reductases (PTGRs), zinc-independent members of the medium-chain dehydrogenase/reductase (MDR) superfamily, perform the first irreversible step of the degradation pathway. We have focused on the characterization of the recombinant human enzyme prostaglandin reductase 1 (PTGR1), also known as leukotriene B₄ dehydrogenase. Only a partial characterization of this enzyme, isolated from human placenta, had been previously reported. Up to now, the enzymatic activity with PGs had been determined by spectrophotometric methods lacking enough sensitivity and reproducibility. In the present work, with the purpose of measuring the PTGR1 activity at submicromolar substrate concentrations, a new HPLC-based method has been validated. We have performed an extensive kinetic characterization of PTGR1, which catalyzes the NADPH-dependent reduction of the α,β -double bond of aliphatic and aromatic aldehydes and ketones, and 15-*keto*-PGs. PTGR1 also shows low activity in the oxidation of leukotriene B₄. The best substrates in terms of k_{cat}/K_m were 15-*keto*-PGE₂, *trans*-3-nonen-2-one and *trans*-2-decenal. Molecular docking simulations, based on the three-

dimensional structure of the human enzyme (PDB ID 2Y05), and site-directed mutagenesis studies were performed to pinpoint important structural determinants, highlighting the role of Arg56 and Tyr245 in 15-*keto*-PG binding. Finally, inhibition analysis was done using non-steroidal anti-inflammatory drugs (NSAIDs) as potential inhibitors.

3.2. Introduction

Prostaglandins, leukotrienes and lipoxins are endogenous lipid mediators involved in a wide range of normally physiological and pathological processes: inflammation, leukocyte chemoattraction and activation, cell growth and survival, smooth muscle contraction, luteolysis, adipocyte differentiation, and vasodilation^{13,22,23,39}. Prostaglandin (PG) metabolism begins with the release of arachidonic acid (AA) from membrane phospholipids by phospholipase A₂, in response to inflammatory stimuli. AA is converted to PGH₂ by cyclooxygenases COX-1 and COX-2. Cell-specific PG synthases convert PGH₂ into a series of PGs, (i.e. PGD₂, PGE₂, PGF₂ and PGI₂), which exert their actions by binding to prostanoid receptors (i.e. DP1-DP2, EP1-EP4, FP and PPAR γ -IP receptors, respectively). EP1-EP4 prostanoid receptors are related with inflammatory and tumorigenic processes³⁹. Leukotriene B₄ (LTB₄) and lipoxin A₄ (LXA₄) are also synthesized from AA. LTB₄ is known as one of the most potent leukocyte chemoattractant and activator and is involved in inflammatory diseases. Lipoxins act within a local inflammatory milieu to dampen neutrophil recruitment and promote resolution. All these metabolites must be degraded rapidly once they have performed their function. For this reason, there is a refined mechanism of catalysis which inactivates these compounds. Prostaglandin reductases (PTGRs) are key enzymes in the irreversible inactivation of these eicosanoids²⁹ and they are zinc-independent members of the medium-chain dehydrogenase/reductase (MDR) superfamily³. The AOR family includes three members: PTGR1, PTGR2 or ZADH1, and PTGR3 or ZADH2²¹. Human PTGR1, PTGR2 and

PTGR3 share only 12% amino acid sequence identity, while PTGR1 and PTGR2 are the most closely related with 37% identity²⁰. The three PTGRs are able to reduce 15-*keto*-PGE₂ to the inactive 13,14-dehydro-15-*keto*-PGE₂, with different tissue specificity²¹.

PTGR1 is an alkenal/one oxidoreductase (AOR) catalyzing the reduction of the double bond of α,β -unsaturated alkenals and ketones. PTGR1 is able to act on the three types of eicosanoids and it has received different names according to the various reactions catalyzed. Thus, the reduction of the 13,14 double bond of 15-*keto*-PGs has been described in different species (chicken²⁶, human^{24,25}, pig⁹, guinea pig²⁷ and rat¹⁴). A similar reaction was also observed towards 15-*keto*-LXA₄, generating 13,14-dihydro-LXA₄²³. Furthermore, the enzyme is capable of carrying out the oxidation of a hydroxyl group of LTB₄ and, for this reason, it is also known as leukotriene B₄ 12-hydroxy-dehydrogenase (LTB₄DH, LTB₄D)^{10,28}. Recently, a new activity has been verified: the double bond reduction of fatty acid nitroalkenes¹³. Finally, the reduction of the double bond is implicated in the activation of some pro-drugs with an antitumor chemotherapeutic role (i.e. CS-670⁵² and hydroxymethylacylfulvene⁴⁹). Kinetic studies on PTGR1 had been reported in various mammals (pig⁹, guinea pig²⁷ and rat^{14,38,52}), but only preliminary characterization studies were performed with the human enzyme^{13,25}.

Up to now, the 15-*keto* prostaglandin reductase activity has been determined by direct and indirect spectrophotometric methods, which show some limitations when using submicromolar concentrations of substrate. Here, a new sensitive HPLC-based, end-point determination method was

designed and validated. This new method was used to characterize the kinetic parameters of PTGR1 towards different 15-*keto*-PGs and 15d-PGJ₂ (see Chapter 2). We also report a complete kinetic characterization of human PTGR1 with LTB₄ and different α,β -unsaturated aldehydes and ketones, including 15-*keto*-PGs. In addition, inhibition analysis is presented using non-steroidal anti-inflammatory drugs (NSAIDs) as potential inhibitors. Finally, by using molecular docking and site-directed mutagenesis, we studied the implication of some active-site residues in the catalytic reaction and inhibitor binding.

3.3. Materials and methods

3.3.1. Protein expression and purification

Human PTGR1 and its mutants (Arg56Ala, Tyr245Ala and Tyr245Phe) were expressed by PCR and ligation-independent cloning into the pNIC28-Bsa4 vector⁶⁰, which allows protein expression with a (His)₆ tag under the control of the T7 RNA polymerase promoter and *lac* operon. For protein expression, *Escherichia coli* BL21(DE3)*pLys* strains transformed with the respective constructs were grown in 5 mL LB medium with 33 µg/mL cloramphenicol and 33 µg/mL kanamycin at 37°C overnight. This culture was used to inoculate 1 L 2×YT medium in the presence of the same antibiotics and was incubated at 37 °C until an OD₆₀₀ of 0.6 was reached. Protein expression was then induced by the addition of 0.1 mM IPTG and cells were grown overnight at 22 °C. Cells were collected by centrifugation (20 min, 12,000×*g*), resuspended with 50 mL of Bind Buffer (20 mM Tris-HCl, 0.5 M NaCl, 5 mM imidazole, pH 8) per liter of cell culture and stored frozen at –20°C until use.

For protein purification, cell lysis was performed by treatment with 1 mg/mL lysozyme, 20 µg/mL DNase and 1 mM of protease inhibitor PMSF (Sigma-Aldrich) followed by 2 cycles of 2-min sonication. The resulting cell homogenate was centrifuged (20 min, 12,000×*g*), cleared through filtration and applied to a 5-mL Hi-Trap™ (GE Healthcare) column using an ÄKTA™ FPLC (GE Healthcare) purification system. The protein was eluted by applying a step-wise gradient of increasing imidazole (5, 60, 100 and 250 mM) concentration. The enzyme eluted at 250 mM imidazole and the

corresponding fractions were collected. The imidazole present in the eluted protein fractions was removed through a PD-10 column (*GE Healthcare*). The proteins including the His tag were stored frozen at -80°C in 200- μL aliquots. To follow the purification process, 1-mL aliquots were collected from each step and analyzed by SDS-polyacrylamide gel electrophoresis or using a microfluidic chip Protein 80 in a Bioanalyzer 2100 (*Agilent Technologies*) apparatus.

3.3.2. Cofactor binding to PTGR1 by quenching of intrinsic fluorescence

NADPH and NADH binding to PTGR1 were followed by measuring quenching of protein fluorescence. Fluorescence experiments were performed in a Cary Eclipse (*Varian*) fluorimeter. The excitation and emission wavelengths were 280 nm and 340 nm, respectively. The spectrofluorimeter cuvette contained 4 μM PTGR1. The protein concentration was determined by the Bradford method while the NADPH or NADH concentration in stock solutions was determined by the absorbance at 340 nm. All fluorescence assays were performed at 25°C , in 100 mM sodium phosphate, pH 7.0. Control experiments, using BSA at the same protein concentration as PTGR1, were performed. The dissociation constant (K_D) value of NADPH for PTGR1 was calculated, after subtracting fluorescence values for control BSA, by adjusting experimental data to the equation for one-site binding $B = B_{\text{max}} \cdot [L] / (K_D + [L])$, using nonlinear regression analysis with the program Grafit 5.0.

3.3.3. Molecular weight determination by gel filtration–HPLC analysis

Molecular weight standards were prepared at 2.5 mg/mL and PTGR1 at 2 mg/mL. Aliquots (2.5 μ L) of each protein were analyzed by HPLC (Waters Alliance 2695). The column (Shodex PROTEIN KW-800 series 8.0 mm ID \times 300 mm) was eluted with mobile phase (50 mM sodium phosphate, 0.3 M NaCl, pH 7.0) at a flow rate of 1.0 mL/min.

3.3.4. Kinetic characterization with α,β -unsaturated aldehydes and ketones

Activities were determined in 100 mM sodium phosphate, pH 7.0, at 25°C using 0.5 mM NADPH as a cofactor in 0.2-cm path length cuvettes, with freshly prepared substrate solutions. All substrates were purchased from Sigma–Aldrich and stock solutions were prepared in ethanol, resulting in a final concentration lower than 3% (v/v) ethanol in the assay mixture. The enzymatic activity was measured in a Cary 400 Bio (Varian) spectrophotometer by following the consumption of NADPH at 340 nm ($\epsilon_{340} = 6220 \text{ M}^{-1}\cdot\text{cm}^{-1}$), except for cinnamaldehyde where the activity was monitored at 365 nm ($\epsilon_{365} = 3510 \text{ M}^{-1}\cdot\text{cm}^{-1}$). Reactions started with the addition of the substrate after 2-min pre-incubation of the enzyme with NADPH. The initial velocities were measured in duplicate with at least five different substrate concentrations and the kinetic constants were calculated using nonlinear regression analysis with the program Grafit 5.0. NADPH and NADH kinetic constants were determined in the presence of 0.1 mM *trans*-

3-nonen-2-one. All reported values are expressed as the mean \pm SE of at least three independent experiments.

3.3.5. Kinetic characterization with prostaglandins and LTB₄ by a novel HPLC-based method

Reaction mixtures were prepared in 100 mM sodium phosphate, pH 7.0, 0.2 mM NADPH or 0.5 mM NADP⁺, and enzyme in glass tubes in 1-mL total volume. Reactions were started by the addition of prostaglandin or LTB₄ (Cayman Chemical) and were incubated at different times and substrate concentrations, at 37°C, to obtain a conversion of substrate to product of 10–30%. Just before ending the reaction, 70 μ L LTB₄ (1 ng/ μ L, in sodium phosphate) for prostaglandins or 50 μ L 15-*keto*-PGE₂ (14 ng/ μ L) for LTB₄ was added as an internal standard. The reaction was stopped by the addition of 2 mL ice-cold ethyl acetate and prostaglandins or LTB₄ were extracted by centrifugation at 1200 rpm for 1.5 min at room temperature. The upper layer (80%) was recovered and evaporated under nitrogen. Three-hundred μ L of mobile phase (acetonitrile/0.1% formic acid in water, 35:65, v/v) were added, and an aliquot (200 μ L) was analyzed by HPLC (Waters Alliance 2695). The column (Symmetry C18 Cartridge, 100 Å, 5 μ m, 3 \times 150 mm) was eluted with mobile phase at a flow rate of 1.5 mL/min. The absorbance was monitored at 230 nm (for 15-*keto*-PGs) and 270 nm (for LTB₄). The specific activity of the enzyme was defined as the amount of the product formed per mg of protein.

3.3.6. Determination of the IC₅₀ value for putative PTGR1 inhibitors

The assays were performed in 100 mM sodium phosphate, pH 7.0, 0.5 mM NADPH and various concentrations of inhibitor compounds (Sigma). After 5-min pre-incubation of the enzyme and cofactor with the inhibitor, reactions started with the addition of *trans*-3-nonen-2-one or 15-*keto*-PGE₂, as a substrate. The enzymatic activity was measured spectrophotometrically or by a novel HPLC-based method, as indicated above. All inhibitors were dissolved in dimethylsulfoxide (DMSO), with a final concentration of 1% or 5% (v/v) DMSO in the inhibition assay mixture. Control assays without inhibitor were performed in 1% or 5% (v/v) DMSO. The IC₅₀ value for each compound was determined using nonlinear regression analysis by the program Grafit 5.0.

3.3.7. Docking simulations

Docking simulations were performed with the program AutoDock 4.2. The ligands were 15-*keto*-PGE₂, indomethacin and niflumic acid and their coordinates were generated by drawing the molecule using Symyx Draw 3.2. To eliminate any potential bond length and bond angle biases in the structure, the ligand was subjected to a full minimization prior to the docking using the PRODRG server (<http://davapc1.bioch.dundee.ac.uk/cgi-bin/prodrng>). The crystal structure of the ternary complex of the human enzyme with NADP⁺ and raloxifene (PDB ID: 2Y05) was used as a model. The inhibitor molecule was removed and the protein structure and the cofactor were kept rigid, while all the torsional bonds in the ligand, except

for all the conjugated double bonds, were set free. Gasteiger united atom partial charges were assigned and polar hydrogen atoms were added by using the Hydrogen module in AutoDock Tools (ADT). The dimensions of the grid were $70 \times 70 \times 70 \text{ \AA}$, with a spacing of 0.375 \AA between the grid points, and centered in the coordinates of the Tyr245 hydroxyl group. The ligand docking was accomplished using 150 Lamarckian genetic algorithms (LGA) from random initial position of the ligand. The docking parameters were left as default. Following docking, all structures generated for the same compound were subjected to cluster analysis with a tolerance of 2.0 \AA for an all-atom root mean square deviation (rmsd) from a lower energy structure. Figures were prepared using PyMOL.

3.4. Results

3.4.1. New HPLC-based method for the determination of 15-*keto* prostaglandin reductase activity

The method here developed allows to directly follow the conversion of 15-*keto*-PGs to their respective products (13,14-dihydro-15-*keto*-PGs), using leukotriene B₄ as an internal standard, as shown by the elution chromatograms (Fig. 12). A similar method was used to follow the conversion of LTB₄ and 15d-PGJ₂.

With the final purpose of testing the robustness of the method, the column was calibrated with 15-*keto*-PGE₂ and statistical tests were performed. To determine the precision, three experiments were performed with different known concentrations of 15-*keto*-PGE₂ and with a sufficiently high number of determinations to reach statistical significance. The mean value, standard deviation and coefficient of variation were calculated. Finally, the solvent extraction efficiency was determined by measuring the area under the substrate peak compared to that of the internal standard. This data is summarized in Table 3.

The better quality of the novel HPLC methodology allowed us to perform the kinetics at lower substrate concentrations (micromolar). As a result the *K_m* values found are, in general, significantly lower than those previously reported using other methodologies (Table 4).

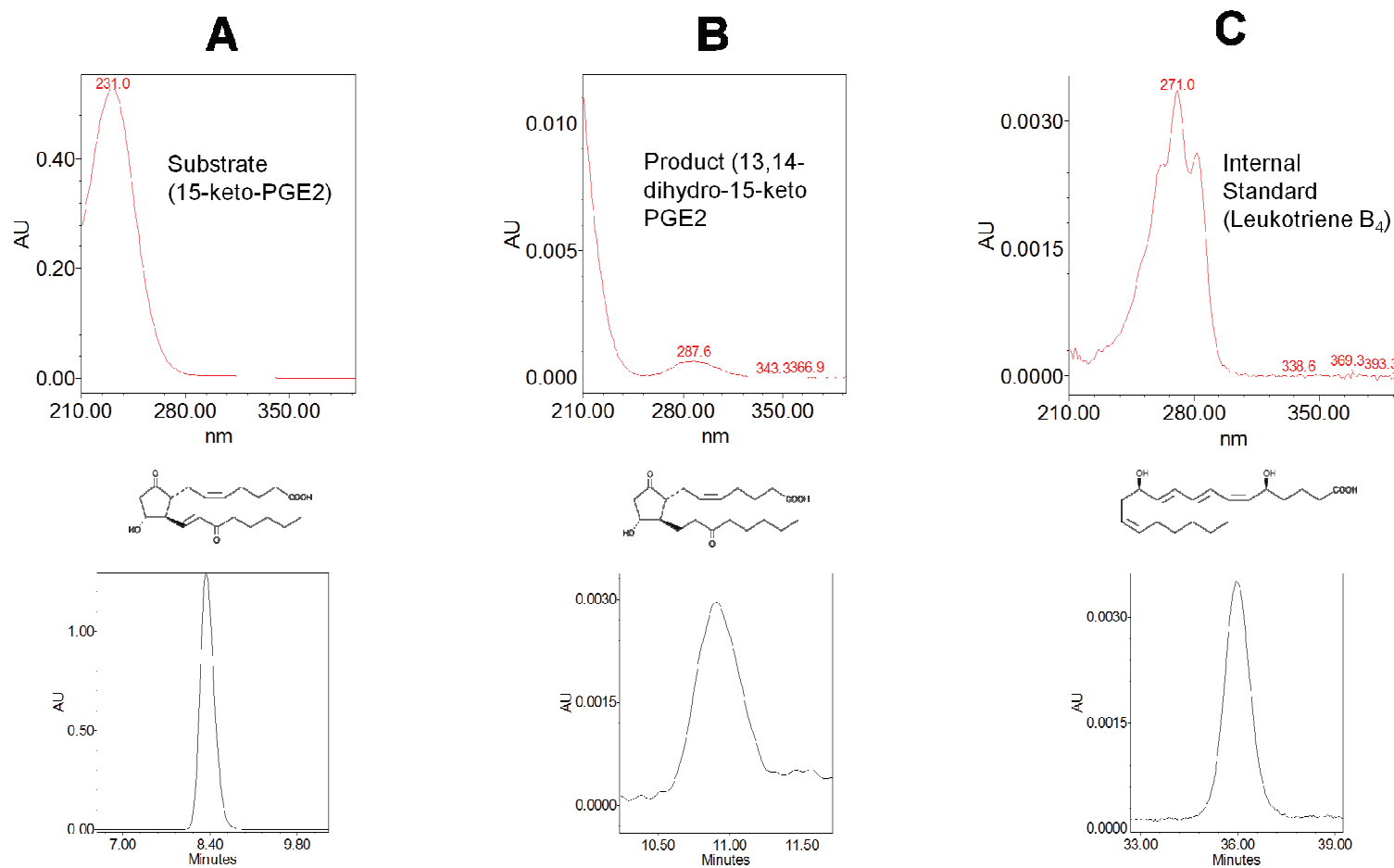


Figure 12: HPLC analysis of prostaglandins and leukotriene B₄. Top: Absorption spectra of prostaglandins and leukotriene B₄. Bottom: Elution profiles from the HPLC column. A: Substrate (15-*keto*-PGE₂). B: Product (13,14-dihydro-15-*keto*-PGE₂). C: Internal standard (Leukotriene B₄).

Table 3. Statistical parameters and solvent extraction efficiency.

| Amount (nmol) injected (number of determinations) | Statistical Parameters | Substrate Area (SA) | Internal Standard Area (ISA) | Ratio SA/ISA | Substrate Extraction Efficiency (%) | Internal Standard Extraction Efficiency (%) |
|--|-----------------------------|------------------------|---------------------------------|-----------------|--|--|
| 2.67 (N=23) | Mean value | 1122316.52 | 169432.83 | 6.64 | 86.1 | 80.1 |
| | Standard Deviation | 54746.72 | 12559.71 | 0.35 | 4.2 | 5 |
| | Coefficient of Variation | 0.05 | 0.07 | 0.05 | 0.05 | 0.06 |
| 0.27 (N=18) | Mean value | 120352.22 | 162001.56 | 0.75 | 92.3 | 76 |
| | Standard Deviation | 7447.71 | 20444.16 | 0.11 | 5.7 | 9.6 |
| | Coefficient of Variation | 0.06 | 0.13 | 0.14 | 0.06 | 0.12 |

Different amounts of 15-*keto*-PGE₂ were tested to calculate statistical parameters and solvent extraction efficiency. The mean coefficient of variation (precision) was 0.1 and the extraction efficiency was higher than 89% for the substrate and remained fairly constant (79%) for the internal standard. Values were extrapolated to other 15-*keto*-PGs used in this work given their high structural similarity and physico-chemical properties.

Table 4. Methods to measure 15-keto-PGs

| Method | | Colorimetric (Hansen) | | | Spectrophotometric | | | HPLC-based (this work) | | |
|--------|--------------------------|--------------------------------------|------------------------------------|---|----------------------------|------------------------------------|---|----------------------------|------------------------------------|---|
| Enzyme | Substrate | K_m (μM) | k_{cat} (min^{-1}) | k_{cat}/K_m ($\text{mM}^{-1}\cdot\text{min}^{-1}$) | K_m (μM) | k_{cat} (min^{-1}) | k_{cat}/K_m ($\text{mM}^{-1}\cdot\text{min}^{-1}$) | K_m (μM) | k_{cat} (min^{-1}) | k_{cat}/K_m ($\text{mM}^{-1}\cdot\text{min}^{-1}$) |
| PTGR1 | 15-keto-PGE ₁ | 8.3 ^a | 84.1 | $1\cdot 10^4$ | 1 ^c | 2400 | $2.4\cdot 10^6$ | 1.4 | 6.3 | $4.6\cdot 10^3$ |
| | 15-keto-PGE ₂ | 18.2 ^a 35 ^b | 30.8 12.3 | $1.7\cdot 10^3$ 352.2 | 7.8 ^d | 210 | $2.7\cdot 10^4$ | 0.6 | 13.5 | $2.19\cdot 10^4$ |

^a Data taken from Ref ⁹. ^b Data taken from Ref ²⁷ ^c Data taken from Ref ¹⁴. ^d Data taken from Ref ⁵².

3.4.2. Cofactor specificity of human PTGR1 and quaternary structure

As judged from the fluorescence analysis of cofactor binding, PTGR1 was highly specific for NADPH ($K_D = 2.2 \mu\text{M}$) and bound NADH much more weakly, as the titration curve could not be distinguished from that obtained with BSA (Fig. 13). Consistently, the K_m value for NADPH was much lower than that for NADH (14 vs. $>200 \mu\text{M}$, Table 5). Gel filtration-HPLC analysis of human PTGR1 showed an M_r value of 65,000 (Fig. 14), while protein chip analysis indicated a 36-kDa subunit (Fig. 15). This suggests that PTGR1 is a dimer like many MDR proteins.

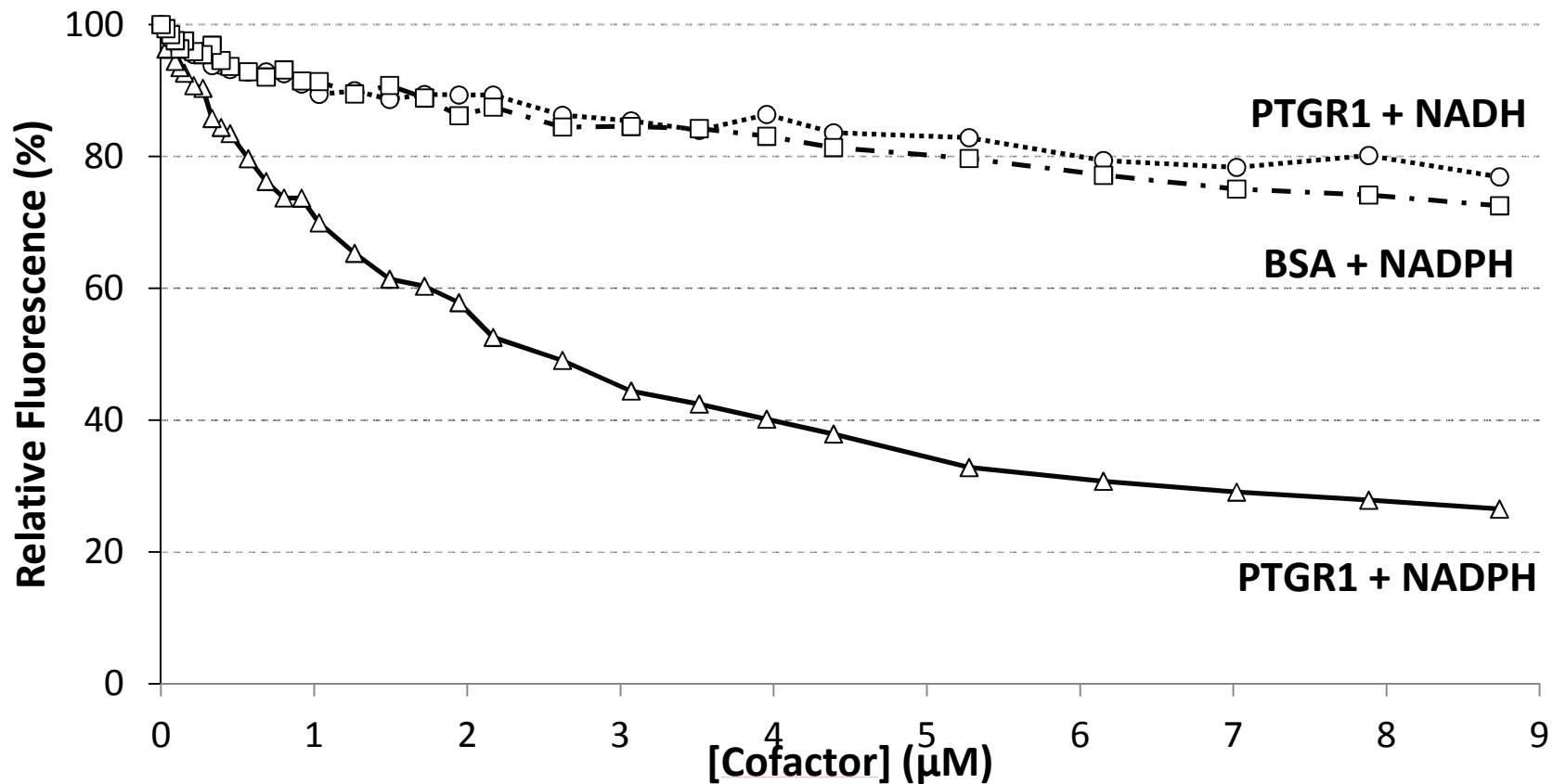


Figure 13: Fluorescence quenching on NADPH and NADH binding to human PTGR1. Change of the protein fluorescence intensity (in percentage) upon addition of cofactor. PTGR1 and bovine serum albumin (BSA) were used at a concentration of 4 μM in 100 mM sodium phosphate, pH 7.0, at 25 °C. Graph symbols: PTGR1 + NADPH (triangles), PTGR1 + NADH (circles), BSA + NADPH (squares).

Table 5Kinetic constants of human PTGR1 with α,β -unsaturated aldehydes and ketones

| Substrate | K_m (μM) | k_{cat} (min^{-1}) | k_{cat}/K_m ($\text{mM}^{-1}\cdot\text{min}^{-1}$) |
|------------------------------|----------------------------|------------------------------------|---|
| <i>Trans</i> -2-hexenal | 33 \pm 6 | 12 \pm 0.6 | 370 \pm 72 |
| <i>Trans</i> -2-octenal | 14 \pm 3 | 46 \pm 3 | 3400 \pm 800 |
| <i>Trans</i> -2-decenal | 6 \pm 2.3 | 42 \pm 3.3 | 7000 \pm 2700 |
| <i>Trans</i> -2-dodecenal | 12 \pm 2.5 | 37 \pm 2 | 3100 \pm 670 |
| Cinnamaldehyde | N.S. | N.S. | 7.6 ^a |
| Acrolein | N.S. | N.S. | 15 ^a |
| 4-Hydroxy-2-hexenal | N.S. | N.S. | 57 ^a |
| 4-Hydroxy-2-nonenal | N.S. | N.S. | 201 ^a |
| <i>Trans</i> -3-buten-2-one | 12 \pm 1.7 | 27.5 \pm 1 | 2200 \pm 340 |
| <i>Trans</i> -3-penten-2-one | 7.3 \pm 1 | 17 \pm 0.5 | 2400 \pm 61 |
| <i>Trans</i> -3-nonen-2-one | 6.5 \pm 0.5 | 61 \pm 1 | 9400 \pm 800 |
| NADPH | 14 \pm 2.6 | – | – |
| NADH | >200 \pm 70 ^b | – | – |

Activity was determined in 0.1 M sodium phosphate, pH 7.0, with 0.2 mM NADPH, at 25°C. NADPH constants were determined with 0.1 mM *trans*-3-nonen-2-one as a substrate. N.S., no saturation. ^a The k_{cat}/K_m values were calculated from the slope of $V/[E]$ versus $[S]$ linear plot. ^b Saturation could not be reached with 4 mM NADH.

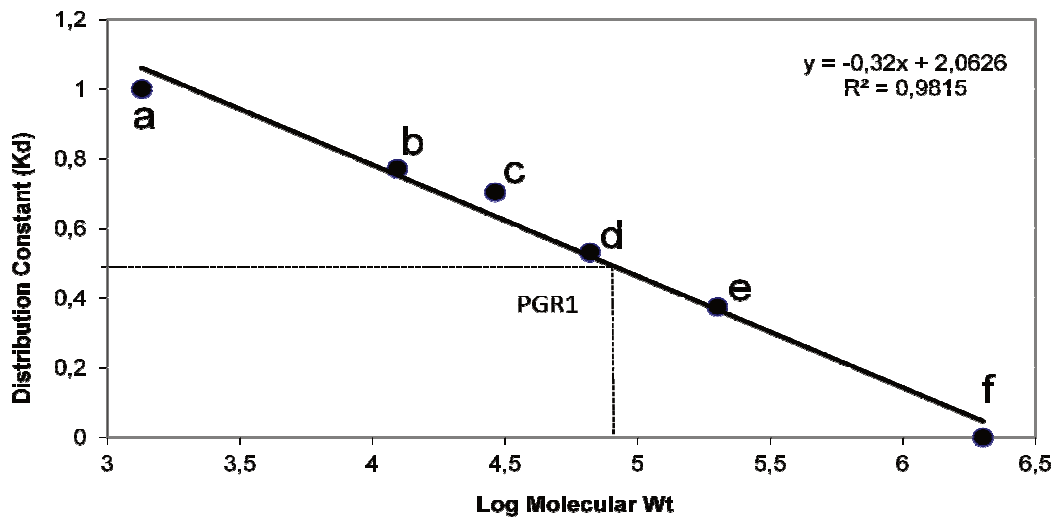


Figure 14: Determination of molecular weight by size exclusion chromatography. Molecular weight standards: (a) Vitamin B12 (1,355), (b) Cytochrome C (12,400), (c) Carbonic Anhydrase (29,000), (d) BSA (66,000), (e) β -Amylase (200,000) and (f) Blue Dextran (2,000,000). $K_d = (V_e - V_o)/(V_t - V_o)$, where V_e =elution volume; V_o =void volume (V_e of Blue Dextran); V_t = volume of packed bed (V_e of vitamin B12).

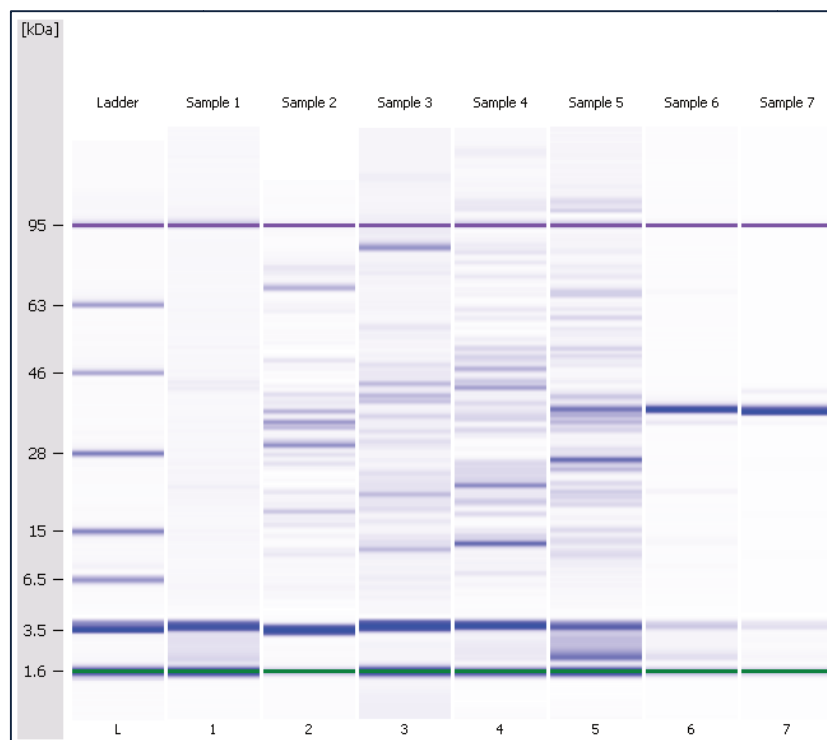


Figure 15: Protein Chip analysis of fractions after affinity chromatography of recombinant human PTGR1. Lanes: L, Agilent Protein 80 Ladder; 1, Pre-induction protein fraction; 2, Post-induction fraction; 3, Flowthrough; 4, Proteins eluted at 5 mM imidazole; 5, Proteins eluted at 60 mM imidazole; 6, Proteins eluted at 100 mM imidazole; 7, Human PTGR1 including the His tag.

3.4.3. Kinetic characterization of human PTGR1 with α,β -unsaturated aldehydes and ketones

Enzymatic activity was assayed with different α,β -unsaturated aldehydes and ketones which included aliphatic and aromatic compounds (Fig. 16), in the presence of NADPH as a cofactor. Some of the compounds assayed were found to be effective substrates for PTGR1 (Table 5). The best aldehyde was *trans*-2-decenal ($k_{\text{cat}}/K_m = 7000 \pm 2700 \text{ mM}^{-1} \text{ min}^{-1}$) and the best ketone was *trans*-3-nonen-2-one ($k_{\text{cat}}/K_m = 9400 \pm 800 \text{ mM}^{-1} \text{ min}^{-1}$). Cinnamaldehyde and the lipid peroxidation products, acrolein (propenal), 4-hydroxy-2-hexenal and 4-hydroxy-2-nonenal, did not saturate the enzyme. The presence of a hydroxyl group in the aliphatic chain leads to an important drop in the catalytic efficiency probably as a consequence of an increase in the K_m value (Table 5). The results indicate that PTGR1 is more efficient catalyzing the reduction of medium-chain aliphatic substrates while it exhibits low activity towards lipid peroxidation products and aromatic substrates.

3.4.4. Kinetic characterization of human PTGR1 with prostaglandins and LTB₄ through a new HPLC-based method

The activity of PTGR1 with different 15-*keto*-prostaglandins and LTB₄ (Fig. 17) was determined by the novel HPLC-based method, which allowed us to perform kinetic assays using substrate concentrations in the lower μM range. The elution chromatograms showed the conversion of 15-*keto*-prostaglandins to their respective 13,14-dihydro-15-*keto*-prostaglandin products, which were identified by their retention times and UV-vis

absorption spectra, using appropriate standards (for a typical 15-*keto*-PGE₂ profile, please see Fig. 18). Likewise, the conversion of LTB₄ to 12-*keto*-LTB₄ was also verified (Fig. 19).

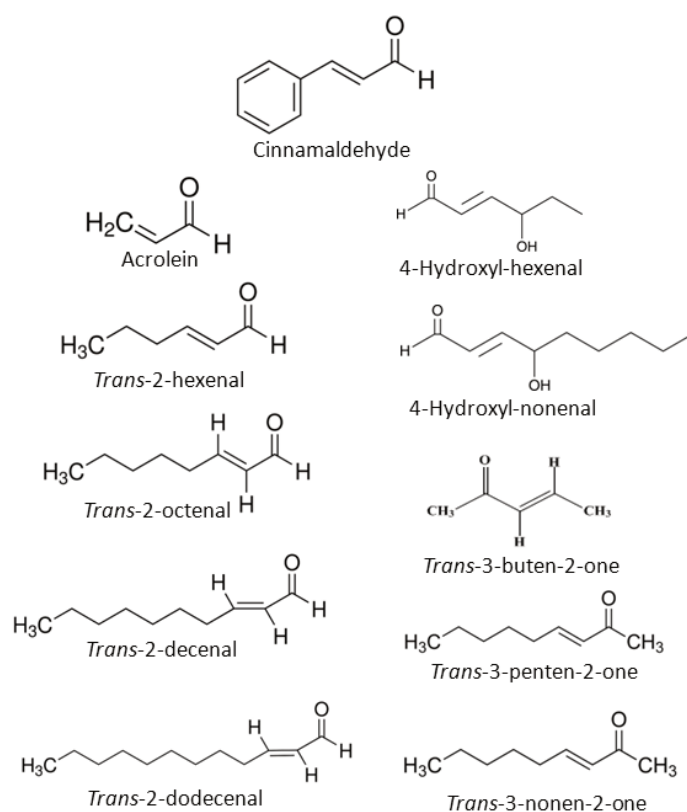


Figure 16: Structures of aliphatic and aromatic compounds.

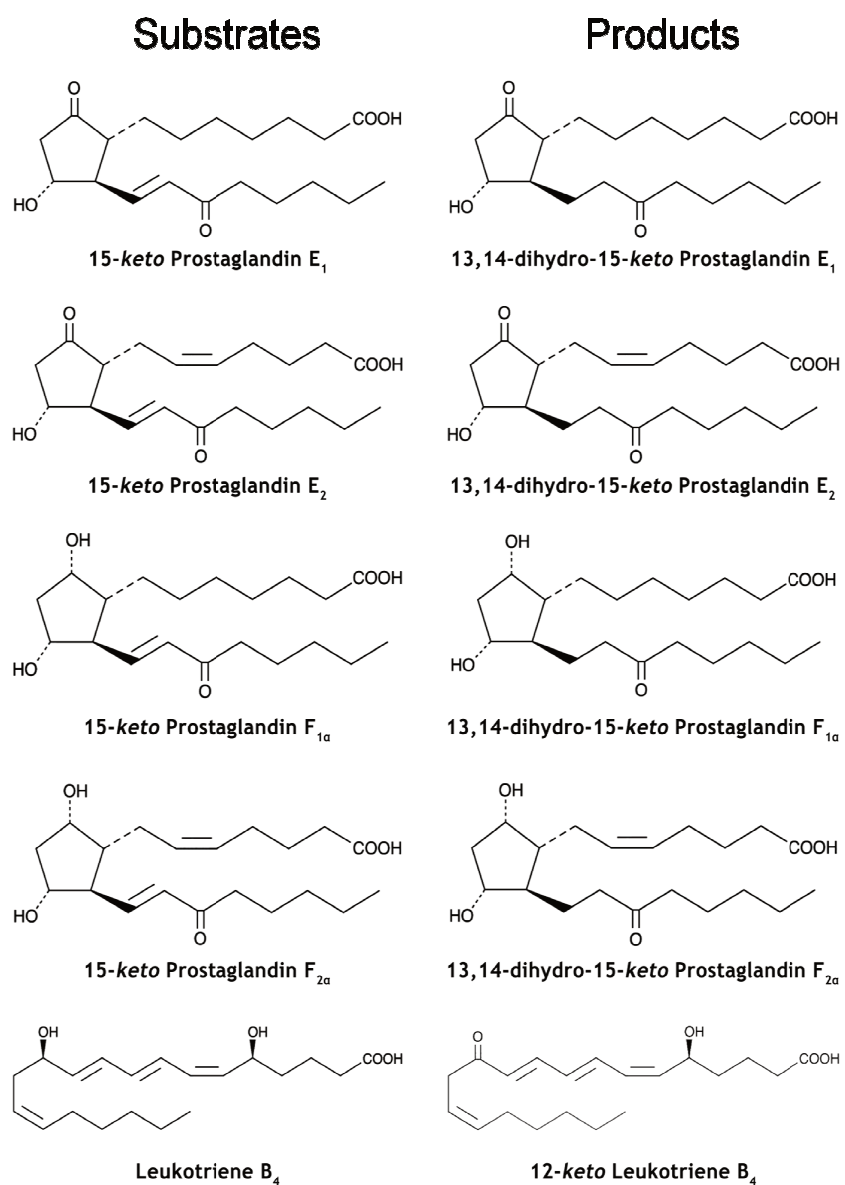


Figure 17: Structures of 15-keto-prostaglandins and leukotriene B₄ used as substrates and their products. Substrates, on the left, and the corresponding products, on the right, after reduction or oxidation by PTGR1.

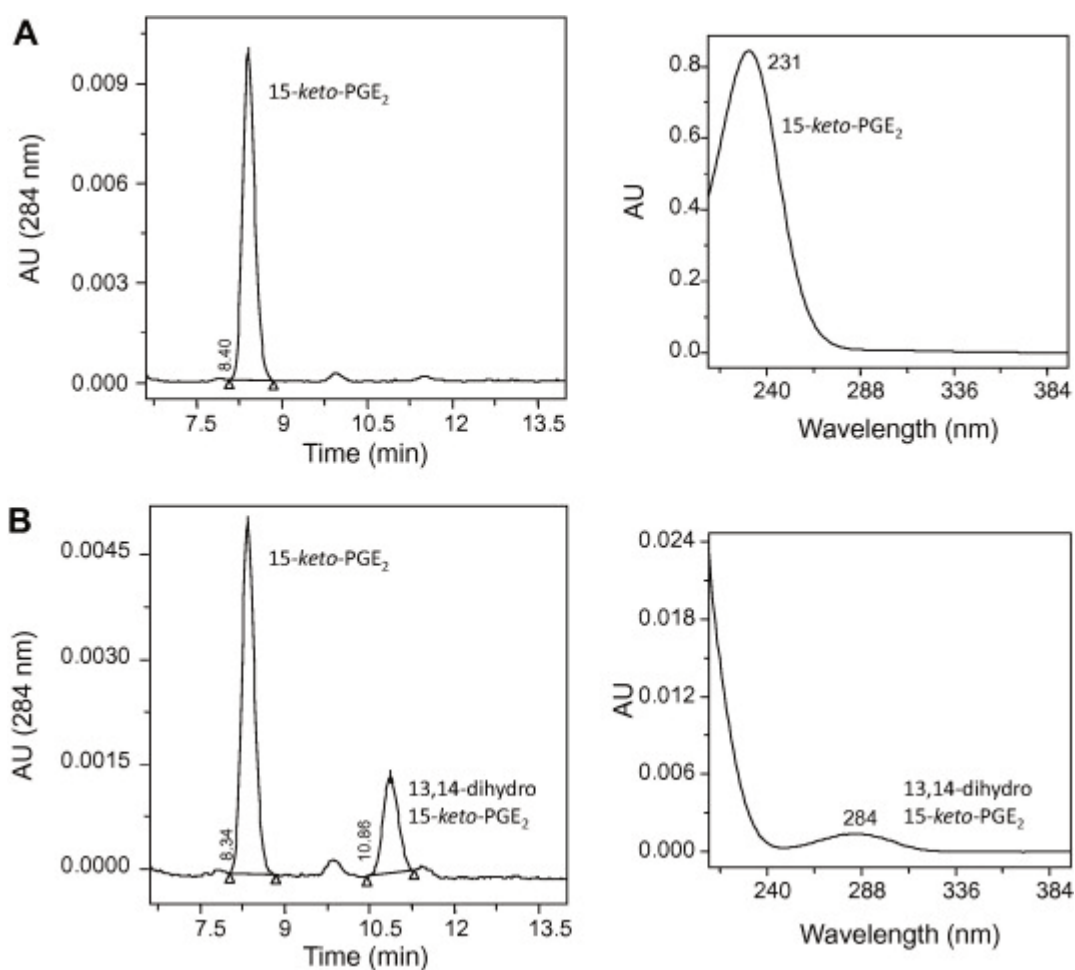


Figure 18: HPLC analysis of the reduction reaction of 15-keto-PGE₂ by PTGR1. (A) No enzyme was added to the reaction mixture. (B) PTGR1 was added. Left: elution profile of substrate and product. Right: UV-vis absorption spectrum of each compound.

The kinetic constants with 15-keto-PGs and LTB₄ are shown in Table 6. PTGR1 showed activity with all the tested prostaglandins, having K_m values near 1 μM , far below those found with non-prostaglandin substrates. In terms of catalytic efficiency, 15-keto-prostaglandin E₂ (15-keto-PGE₂) was the best substrate, with the lowest K_m and the highest k_{cat}/K_m (21,900 $\text{mM}^{-1} \text{min}^{-1}$) values. It should be noticed that the K_m values here determined are in general significantly lower than those previously reported for PTGR1 from other species using different methodologies (Table 7). PTGR1 also oxidized LTB₄ but with a much lower catalytic efficiency. The k_{cat}

values were similar or similar than those for PTGR1 from other species (Table 7).

Table 6. Kinetic parameters of human PTGR1 with prostaglandins and leukotriene B₄.

| Substrate | K_m (μM) | k_{cat} (min^{-1}) | k_{cat}/K_m ($\text{mM}^{-1}\cdot\text{min}^{-1}$) |
|--|----------------------------|------------------------------------|---|
| 15- <i>keto</i> -PGE ₁ | 1.4 ± 0.3 | 6.3 ± 0.4 | 4600 ± 1000 |
| 15- <i>keto</i> -PGE ₂ | 0.6 ± 0.2 | 13.5 ± 1.1 | 21900 ± 6600 |
| 15- <i>keto</i> -PGF _{1α} | 1.1 ± 0.3 | 4.4 ± 0.2 | 2000 ± 1000 |
| 15- <i>keto</i> -PGF _{2α} | 3.2 ± 0.9 | 5.1 ± 0.4 | 1600 ± 460 |
| LTB ₄ | 5.2 ± 1.4 | 0.17 ± 0.02 | 32 ± 9 |

Activity was determined in 0.1 M sodium phosphate, pH 7.0 at 37°C, with 0.2 mM NADPH for prostaglandins or 0.5 mM NADP⁺ for leukotriene B₄.

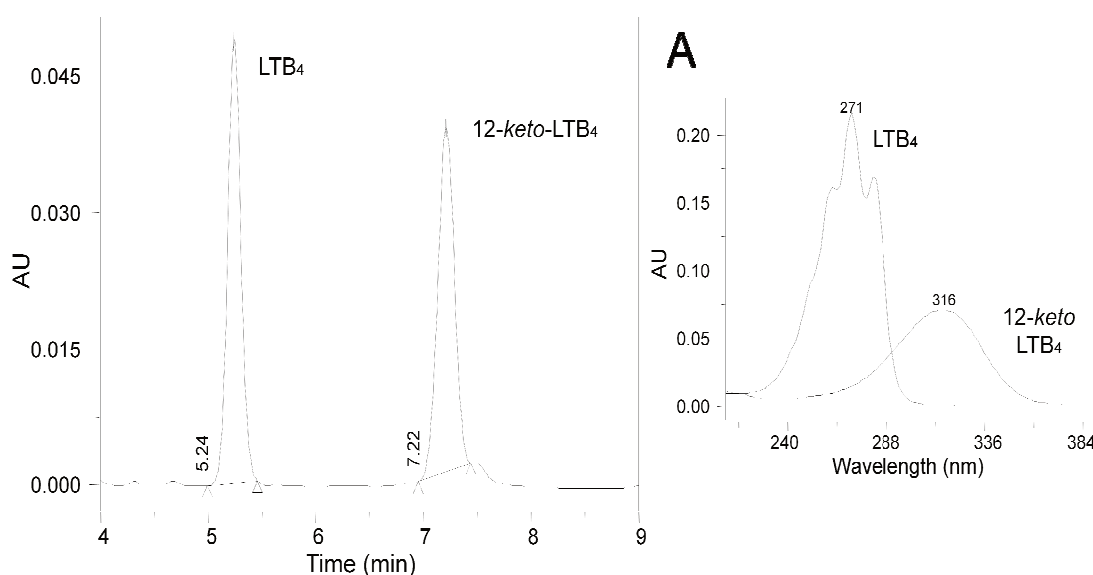


Figure 19: Chromatogram LTB₄ and 12-keto-LTB₄. Chromatographic profile at 290nm showing separation of individual LTB₄ and their metabolite, 12-keto-LTB₄. A: UV-vis absorption spectrum of each compound.

Table 7Comparison of kinetic constants of mammalian PTGR1 enzymes towards prostaglandins and leukotriene B₄

| Substrate | Human | | | Guinea-pig ^a | | | Pig ^b | | | Rat | | |
|---------------------------------|----------------------------|------------------------------------|---|----------------------------|------------------------------------|---|----------------------------|------------------------------------|---|----------------------------|------------------------------------|---|
| | K_m (μM) | k_{cat} (min^{-1}) | k_{cat}/K_m ($\text{mM}^{-1}\cdot\text{min}^{-1}$) | K_m (μM) | k_{cat} (min^{-1}) | k_{cat}/K_m ($\text{mM}^{-1}\cdot\text{min}^{-1}$) | K_m (μM) | k_{cat} (min^{-1}) | k_{cat}/K_m ($\text{mM}^{-1}\cdot\text{min}^{-1}$) | K_m (μM) | k_{cat} (min^{-1}) | k_{cat}/K_m ($\text{mM}^{-1}\cdot\text{min}^{-1}$) |
| <i>15-keto-PGE</i> ₁ | 1.4 ± 0.3 | 6.3 ± 0.4 | 4600 ± 1000 | N.D. | N.D. | N.D. | 8.3 | 84.1 | 1·10 ⁴ | 1 ^c | 2400 | 2.4·10 ⁶ |
| <i>15-keto-PGE</i> ₂ | 0.6 ± 0.2 | 13.5 ± 1.1 | 21900 ± 6600 | 35 | 12.3 | 352.2 | 18.2 | 30.8 | 1.7·10 ³ | 7.8 ^d | 210 | 2.7·10 ⁴ |
| LTB ₄ | 5.2 ± 1.4 | 0.17 ± 0.02 | 32 ± 9 | 93 | 0.06 | 0.65 | 10 | 0.3 | 30 | 0.028 ^e | 0.3 | 10000 |

N.D., not determined. ^a Data taken from Ref ²⁷. ^b Data taken from Ref. ⁹. ^c Data taken from Ref. ¹⁴. ^d Data taken from Ref. ⁵². ^e Data taken from Ref. ⁵⁰.

3.4.5. Docking simulations of 15-*keto*-prostaglandin E₂ to PTGR1

To gain some insight on how 15-*keto*-PGE₂ may bind to PTGR1, this substrate was docked into the active site of the human holoenzyme (PDB ID 2Y05, Fig. 20). The resulting docking model was also superimposed to the holoenzyme structure of guinea-pig PTGR1 bound to 15-*keto*-PGE₂ (PDB ID 1V3V)²⁹, although the cyclopentane ring and the carboxyl group side chain were not observed in the crystal. 15-*keto*-PGE₂ can be accommodated into the substrate-binding site of human PTGR1 with a favorable binding energy ($\Delta G = -6.3$ kcal/mol). In the model, the conformation of the omega chain (from C12 to C20) of 15-*keto*-PGE₂ is very similar to that found in the crystallographic structure of the guinea-pig enzyme (Fig. 20). This allowed us to predict a previously undetected ionic interaction between the substrate carboxyl group and Arg56. Residues involved in van der Waals interactions were Tyr49, Val52, Tyr245, Glu258, Ile261, Tyr262, Val272 and Tyr273 (Fig. 20). Residues Tyr49, Tyr245, Glu258, Ile261, Tyr262 and Val272 are strictly conserved in all species where kinetic studies have been performed (Fig. 21). Furthermore, while Arg56 is not fully conserved, the corresponding residue found in rat and pig sequences is Lys, which is positively charged like Arg. It is noteworthy that Tyr245 (fully conserved among human PTGR1, PTGR2 and PTGR3) interacts through a hydrogen bond with the 2'-hydroxyl group of the NADPH ribose, which in turn interacts with the 15-*keto* group of the substrate (Fig. 20), similarly as observed in the guinea-pig PTGR1 structure²⁹.

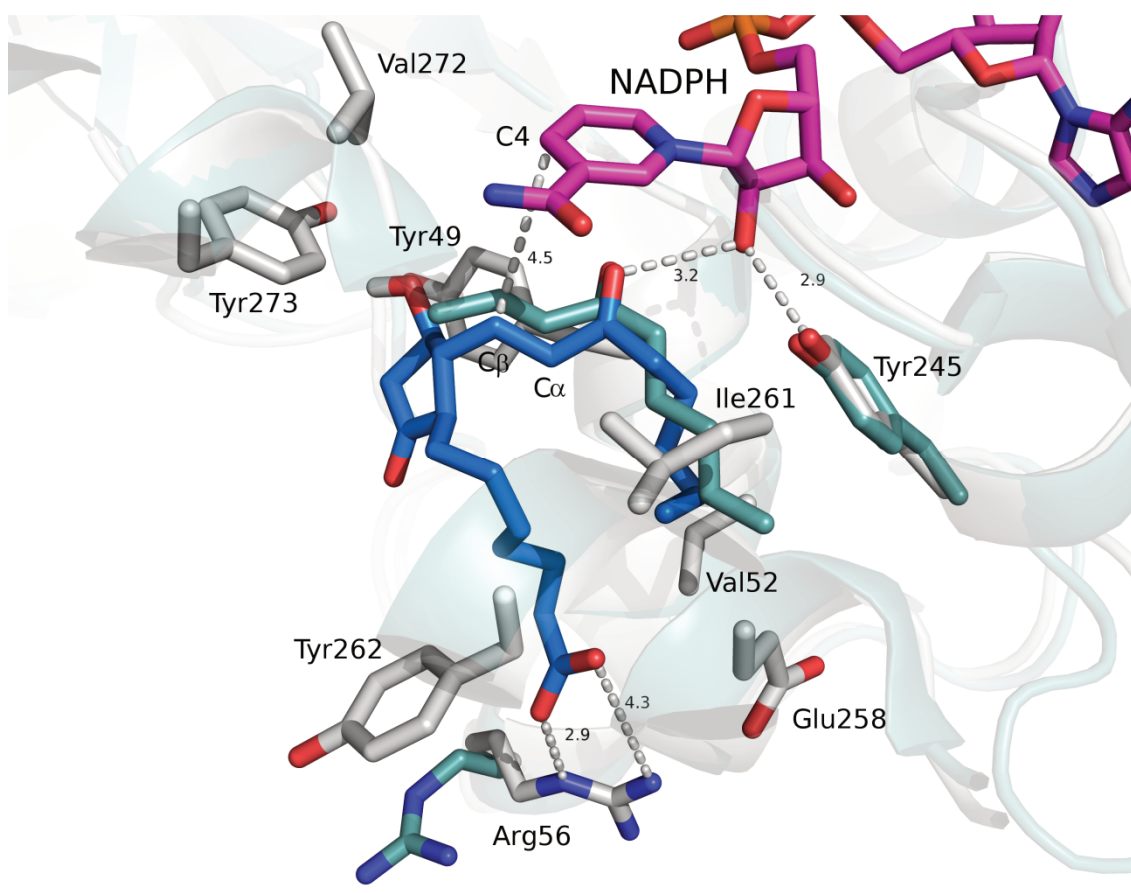


Figure 20: Docking simulation of 15-keto-PGE₂ bound into the PTGR1 active site.

The structure of guinea-pig PTGR1 in ternary complex with NADP⁺ and 15-keto-PGE₂ (PDB ID 1V3V), in green, was superimposed to the human PTGR1 structure (PDB ID 2Y05), in gray. The docking was performed with 15-keto-PGE₂ on human PTGR1. The carbonyl group of the α,β -unsaturated aliphatic chain interacts with the 2'-hydroxyl group of the nicotinamide ribose through a hydrogen bond (3.2 Å). Tyr245 also forms a hydrogen bond with the 2'-hydroxyl group of the nicotinamide ribose (2.9 Å). The distance between the C4 atom of the nicotinamide and C β of the substrate is shown. A predicted ionic interaction between Arg56 and the substrate carboxyl group is depicted. Residues involved in van der Waals interactions are shown: Tyr49, Val52, Tyr245, Glu258, Ile261, Tyr262, Val 272 and Tyr273.

| | | | | |
|-----|---|-----|--------|------------------|
| 1 | MVRTKTWTLKKHFVGYPTNSDFELKTAELPPLKNGEVLLLEALFLTVDPPMRVAAKRLKEG | 60 | Q14914 | PTGR1_HUMAN |
| | MVKAKSWTLKKHFQKQPTQSDFELKTVELPPLKNGEVLLLEALFLSVDPPMRIAASKRLKEG | 60 | Q9EQZ5 | PTGR1_GUINEA-PIG |
| | MVRAKSWTLKKHFVGYPTPSNFELKTVELPPLKNGEVLLLEALFLTVDPPMRIAARKLKEG | 60 | Q29073 | PTGR1_PIG |
| | MVQAKTWTLLKKHFEFGPTDSNFELRTELEPPLNNGEVLLLEALFLSVDPPMRVAAKRLKEG | 60 | P97584 | PTGR1_RAT |
| | *:.*:***** * ** *:*:*:*.*:*****:*****:*****:*.:.**** | | | |
| 61 | DTMMGQQVAKVVESKNVALPKGTIVLASPGWTTTHSISDGKDKLEKLLTEWPDITPLSLALG | 120 | Q14914 | PTGR1_HUMAN |
| | AVMMGQQVARVVESKNSAFPAGSIVLAQSGWTTTHFISDGKDKLEKLLTEWPKLPLSLALG | 120 | Q9EQZ5 | PTGR1_GUINEA-PIG |
| | DMMMGEQVARVIESKNAAFPPTGTIVVALLGWTTHSISDGKNLERLLAEWPDITPLSLTLG | 120 | Q29073 | PTGR1_PIG |
| | DSMMGEQVARVVESKNSAFPPTGTIVVALLGWTSHSISDGNLRLKLPAEWPKLPLSLALG | 120 | P97584 | PTGR1_RAT |
| | ***:***:*.**** *:* *:*:* ***: * ***: *.:. * :****:****:*** | | | |
| 121 | TVGMPGLTAYFGLLEICGVKGGETVMVNAAGAVGSVVGQIAKLGCKVVGAVGSDEKVA | 180 | Q14914 | PTGR1_HUMAN |
| | TIGMPGLTAYFGLLEICGVKGGETVLVSAAGAVGSVVGQIAKLGCKVVGAVGSDEKVA | 180 | Q9EQZ5 | PTGR1_GUINEA-PIG |
| | TVGMPGLTAYFGLLDICGLKGGETVMVNAAGAVGSVVGQIAKLGCKVVGAVGSDEKVA | 180 | Q29073 | PTGR1_PIG |
| | TVGMPGLTAYFGLLDICGLKGGETVLVNAAGAVGSVVGQIAKLGCKVVGAVGSDEKVA | 180 | P97584 | PTGR1_RAT |
| | *:*****:*.****:*.*****:*****:*****:*****:*****:* | | | |
| 181 | YLKQIGFDVAFNYKTIESLEETLKKASPDGYDCYFDNVGGEFSNTVIGQMKKFGRIAICG | 240 | Q14914 | PTGR1_HUMAN |
| | YLKQIGFDVAFNYKTIESLEELKASPDGYDCYFDNVGGEFLNTVLSQMKDFGKIAICG | 240 | Q9EQZ5 | PTGR1_GUINEA-PIG |
| | CLKKYGFDAFNYKTIESLEETLKKASPEGYDCYFDNVGGEFSNAVTSQMKKFGRIAICG | 240 | Q29073 | PTGR1_PIG181 |
| | YLKQIGFDVAFNYKTIESLEELRTASPDGYDCYFDNVGGEFSNTVILQMKTFGRIAICG | 240 | P97584 | PTGR1_RAT |
| | *:.* ***.*****:*****:*.****:*****:***** *:* ** ***:***** | | | |
| 241 | AISTVNRGTGPPPPPPPIVTVQELRMEAFVYRWQGDARQKALDKLLKVVLEGKIQYKE | 300 | Q14914 | PTGR1_HUMAN |
| | AISVNRMDQLPPGPPSPSIIYKQLRIEGFIYRWQGDVREKALRDLKVVLEGKIQYHE | 300 | Q9EQZ5 | PTGR1_GUINEA-PIG |
| | AISTVNRGTGPPPPPPPPPIVTVNELCFQGFIVRWQGEVVRQKALRDLKVVLEGKIQYHE | 300 | Q29073 | PTGR1_PIG |
| | AISQNRGTGPPPPPPPIVTVQQLRMEGFIYRWQGEVVRQKALTDLMNWNVSEGKIRYHE | 300 | P97584 | PTGR1_RAT |
| | *** ** * ** * ** * ** * ** * ** * ** * ** * ** * ** * ** * ** * | | | |
| 301 | YIEGFENMPAAFMGMLKGDNLGKTIVKA | 329 | Q14914 | PTGR1_HUMAN |
| | HVTKGFENMPAAFIEMLNGANLGKAVVTA | 329 | Q9EQZ5 | PTGR1_GUINEA-PIG |
| | HITTEGFENMPAAFMGMLKGENLGKAIVKA | 329 | Q29073 | PTGR1_PIG |
| | YITEGFENMPAAFMGMLKGDNLGKTIVKA | 329 | P97584 | PTGR1_RAT |
| | :::***:*****: **:* ***:**:* | | | |

Figure 21: Alignment of PTGR1 amino acid sequences. In the human PTGR1 docking, proposed residues involved in van der Waals interactions with 15-keto-PGE₂ were strictly conserved, such as Tyr49, Tyr245, Glu258, Ile261, Tyr262 and Val 272 (in green), or partially conserved, such as Val52 and Tyr273 (in yellow). Also an ionic interaction with Arg56 (in blue) was predicted.

3.4.6. Kinetic characterization of human PTGR1 mutants Arg56Ala, Tyr245Phe and Tyr245Ala

To empirically support the interactions shown by docking analysis, three mutants were prepared: Arg56Ala, Tyr245Phe and Tyr245Ala. Kinetic analysis was performed with 15-*keto*-PGE₂, *trans*-3-nonen-2-one and NADPH (Table 8).

Table 8

Kinetic parameters of the PTGR1 mutants

| Enzyme | Substrate | | | | | | NADPH <i>K_m</i> (μ M) |
|-----------|---|--|--|------------------------------------|--|--|---|
| | 15- <i>keto</i> -prostaglandin E ₂ | | | <i>trans</i> -3-nonen-2-one | | | |
| | <i>K_m</i> (μ M) | <i>k_{cat}</i> (min ⁻¹) | <i>k_{cat}/K_m</i> (mM ⁻¹ ·min ⁻¹) | <i>K_m</i> (μ M) | <i>k_{cat}</i> (min ⁻¹) | <i>k_{cat}/K_m</i> (mM ⁻¹ ·min ⁻¹) | |
| Wild Type | 0.6±0.2 | 13.5±1.1 | 21900±6600 | 6.5±0.5 | 61±1 | 9400±800 | 14±2.6 ^b |
| Arg56Ala | 5.7±1.5 | 7±0.7 | 1230±350 | 6.2±1.9 | 43.9±3.4 | 7108±2256 | 8.9±1.6 ^b |
| Tyr245Phe | 45±6.7 | 57±4.2 | 1270±210 | 116±27 ^a | 70±4 | 600±140 | 19±4 ^c |
| Tyr245Ala | N.D. | N.D. | N.D. | N.S. ^a | N.S. | 9.7 ^d | N.D. |

Activity was determined in 0.1 M sodium phosphate, pH 7.0, with 0.2 mM NADPH unless otherwise stated, at 37°C (15-*keto*-PGE₂) or 25°C (*trans*-3-nonen-2-one). N.D., not determined. N.S., no saturation. ^a 2 mM NADPH was used as a cofactor. ^b 0.2 mM *trans*-3-nonen-2-one was used as a substrate. ^c 2 mM *trans*-3-nonen-2-one was used as a substrate. ^d The *k_{cat}/K_m* value was calculated from the slope of V/[E] versus [S] linear plot.

The Arg56Ala mutant kept the same kinetic parameters towards *trans*-3-nonen-2-one as the wild-type enzyme, but it showed a dramatic decrease in the catalytic efficiency with 15-*keto*-PGE₂. These results support the prediction by docking simulations. Thus, Arg56 is relevant for the

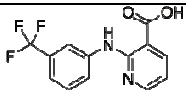
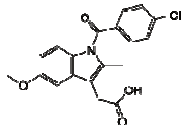
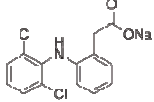
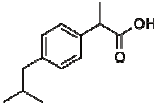
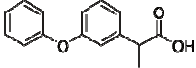
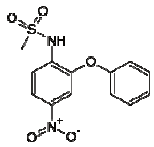
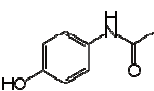
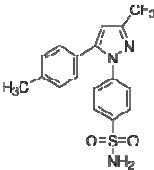
binding of 15-*keto*-PGs substrates through anchoring the side chain carboxyl group.

With 15-*keto*-PGE₂ and *trans*-3-nonen-2-one, the Tyr245Phe mutant showed a notable decrease in the catalytic efficiency as a consequence of the rise in the K_m values, while k_{cat} values did not decrease. Furthermore, the Tyr245Ala mutant displayed an important increase in the K_m value towards *trans*-3-nonen-3-one (indeed, the enzyme did not saturate), suggesting that Tyr245 is involved in substrate binding.

3.4.7. Inhibition of human PTGR1 by classical inhibitors of prostaglandin metabolism

The compounds evaluated in this study as PTGR1 inhibitors were synthetic drugs, classified as NSAIDs, except for acetaminophen (Table 9). The agents with the highest inhibitory potency were niflumic acid and indomethacin, with IC₅₀ values of 7.1 ± 1.3 and 8.7 ± 0.8 μ M, respectively. It is important to note that indomethacin had been previously tested against guinea-pig PTGR1 (IC₅₀ = 97.9 ± 19.4 μ M)³⁰. Diclofenac also provided inhibition, although with a threefold higher IC₅₀ value. Ibuprofen, fenoprofen and nimesulide displayed low inhibitory potency, with IC₅₀ values higher than 200 μ M. Finally, no inhibition was detected with acetaminophen and celecoxib.

Table 9IC₅₀ values for compounds assayed as inhibitors against PTGR1

| Inhibitor | Structure | IC ₅₀ (μM) |
|---------------|---|-----------------------|
| Niflumic acid |  | 7.1 |
| Indomethacin |  | 8.7 |
| Diclofenac |  | 26 |
| Ibuprofen |  | >200 |
| Fenoprofen |  | >200 |
| Nimesulide |  | >200 |
| Acetaminophen |  | N.I. |
| Celecoxib |  | N.I. |

Activity was measured in 0.1 M sodium phosphate, pH 7.0, with 0.2 mM NADPH at 25°C. IC₅₀ constants were determined with 100 μM *trans*-3-nonen-2-one as a substrate and a PTGR1 concentration of 400 nM. N.I., no inhibition.

3.4.8. Docking simulations of indomethacin and niflumic acid to PTGR1

With the aim to obtain structural information on the binding of the inhibitors to the PTGR1 binding pocket, docking simulations were performed using indomethacin and niflumic acid as ligands (Fig. 22). It appears that these inhibitors bind in a fairly similar way, by occupying the active-site pocket. Thus, both displayed an ionic interaction between their carboxyl groups and Arg56, as it has been described above in the binding of 15-*keto*-PGE₂. It is important to note that Arg56 was previously proposed as relevant for inhibitor binding in guinea-pig PTGR1, which was structurally solved in complex with indomethacin (PDB ID 2DM6)³⁰. It is remarkable that the hydroxyl group of Tyr262 adopts a different orientation in the human and guinea-pig structures, which makes the indomethacin position to be quite different between the two enzymes (Fig. 23). In order to investigate the role of Arg56 in inhibitor binding, inhibition studies were performed with the Arg56Ala mutant under different conditions and using different substrates (Table 10). Results showed significant differences only for niflumic acid, in good agreement with losing the ionic interaction with Arg56. This difference between the two inhibitors could be rationalized in terms of the higher flexibility of indomethacin^{30,61}. It is conceivable that indomethacin might be able to adapt its conformation in the mutated enzyme, by finding alternative interactions.

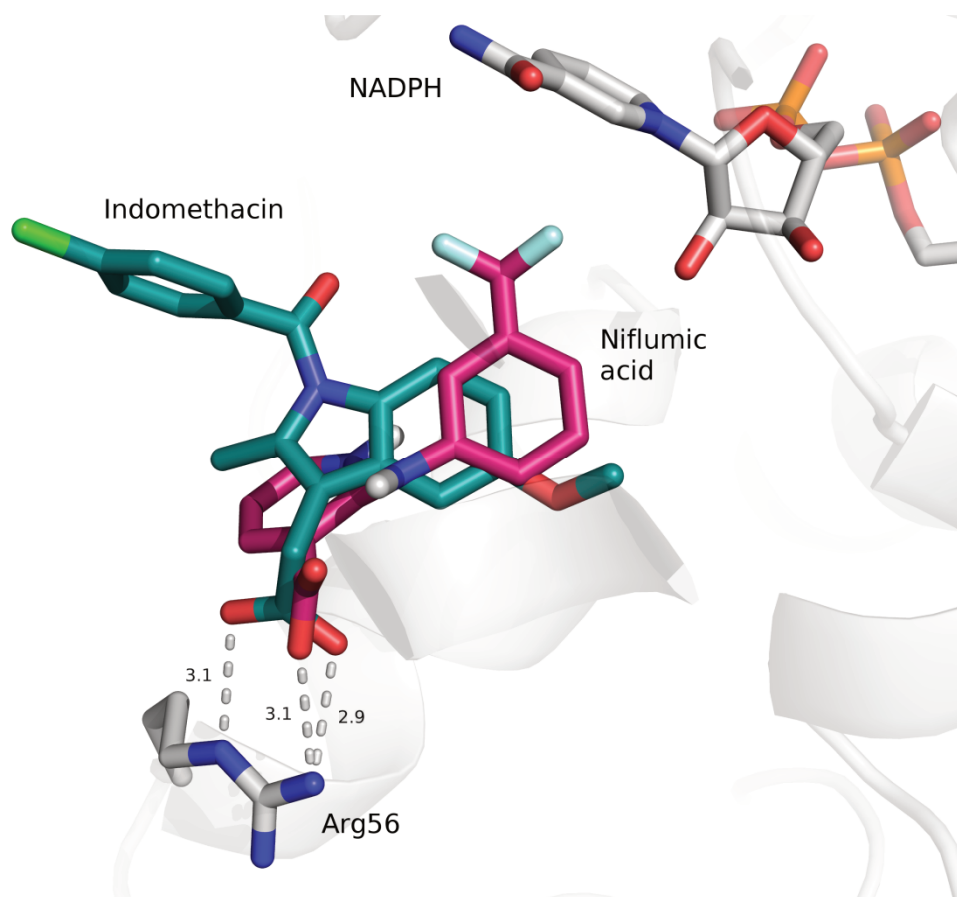


Figure 22: Docking simulation of inhibitors on the active-site pocket of PTGR1.

The binding mode of indomethacin (green) and niflumic acid (pink) are shown, according to the molecular docking analysis. A predicted ionic interaction between Arg56 and the inhibitor carboxyl group is depicted.

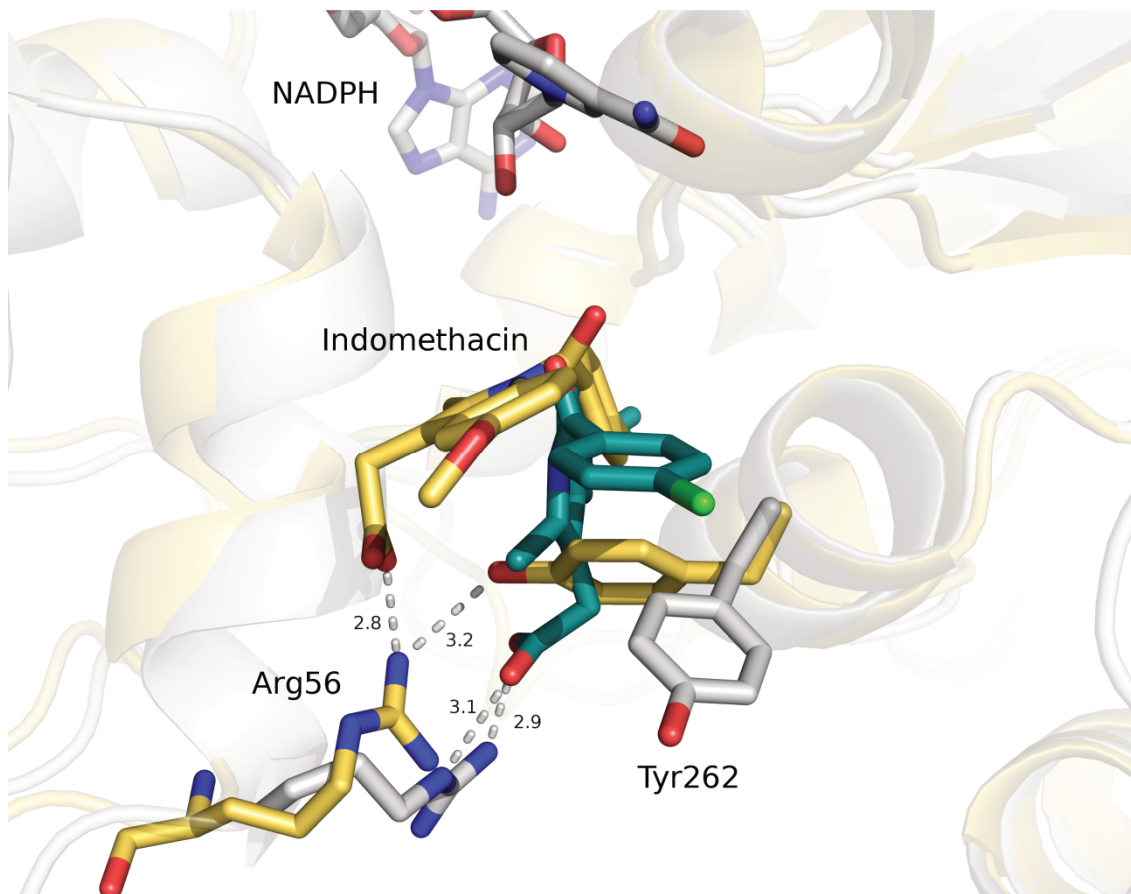


Figure 23: Superimposition of indomethacin bound to the active-site pocket of guinea-pig and human PTGR1.

The structure of guinea-pig PTGR1 in ternary complex with NADP⁺ and indomethacin (PDB ID 2DM6), in yellow, was superimposed to the human PTGR1 structure (PDB ID 2Y05), in gray. The docking of indomethacin to human PTGR1 is shown in green.

Table 10

IC₅₀ values (μM) with wild-type PTGR1 and the Arg56Ala mutant

| Inhibitor | Wild type | Arg56Ala |
|---------------|------------------------|------------------------|
| Indomethacin | 8.7 ± 0.8 ^a | 7.8 ± 1.7 ^a |
| | 3.6 ± 2.3 ^b | 5.8 ± 1.3 ^b |
| | 3.2 ± 0.4 ^c | 2.2 ± 1.8 ^c |
| Niflumic acid | 7.1 ± 1.3 ^a | 17 ± 6 ^a |
| | 3.7 ± 1.8 ^b | 12 ± 4 ^b |

Activity was measured in 0.1 M sodium phosphate, pH 7.0, with 0.2 mM NADPH. IC₅₀ values were determined with: ^a100 μM *trans*-3-nonen-2-one as a substrate, 5% (v/v) DMSO and 400 nM PTGR1, at 25°C; ^b20 μM *trans*-3-nonen-2-one as a substrate, 1% DMSO and 400 nM PTGR1, at 25°C; ^c16 and 20 μM 15-*keto*-PGE₂ as a substrate (for wild-type and Arg56Ala, respectively), 1% (v/v) DMSO and 30 nM PTGR1, at 37°C.

3.5. Discussion

This work provides the most extensive kinetic characterization for human PTGR1. Previously, in the 70s, some authors worked with the enzyme purified from human placental tissue. In these early reports, the reduction of the 13,14 double bond in some 15-*keto*-PGs was described using NADH as a cofactor^{24,25}. Our results show clearly that PTGR1 uses preferentially NADPH instead of NADH (Figure 13 and Table 5). Human PTGR1 can reduce efficiently α,β -unsaturated aldehydes and ketones, especially those with medium-chain length (8–12 carbons). However, the human enzyme catalyzes with low efficiency the reduction of some lipid peroxidation products (e.g. 4-hydroxy-2-hexenal and 4-hydroxy-2-nonenal), in contrast to rat PTGR1¹⁴, despite their high amino acid sequence identity.

The new HPLC-based method is robust and quantitative, with good reproducibility and precision. Table 4 compares the new method with the indirect colorimetric method of Hansen⁶² and the direct spectrophotometric method^{14,52}. In general, our method yields lower K_m values, although comparisons are difficult because kinetic constants were obtained with enzymes from different species. The HPLC-based method has several advantages over previous methods, regarding sensitivity and reliability, as it allows the identification of the actual reaction products by using appropriate standards when available. As a result, lower substrate concentrations can be used in the assay and more reliable K_m values at micromolar to submicromolar levels can be obtained. With the aim to measure the steady-state enzymatic activity, the concentration of enzyme

was kept from 25- to 100-fold lower than that of the substrate for all the enzymatic assays.

PTGR1 showed 15-*keto*-PGs to be the best substrates (Table 6), corroborating that the enzyme is involved in the physiological metabolism of PGs. The here determined K_m values are significantly lower than those previously reported for PTGR1 from other species^{9,14,27,38,52} (Table 7). The new HPLC-based method allows performing kinetic assays at lower μM concentration of substrate in comparison with other methods (Table 4) and, therefore, it could explain at least partially the low K_m values. The low oxidative activity with LTB_4 , and considering the cellular NADPH/NADP⁺ ratios, suggests that the main physiological role of PTGR1 would be the reduction of 15-*keto*-PGs.

In addition, this work provides a structural study of the residues involved in the catalysis/binding of the substrate. Previously, it was described the structure of guinea-pig PTGR1 in complex with 15-*keto*- PGE_2 ²⁹. However, the aliphatic side chain with the terminal carboxylic group could not be solved in this structure (PDB ID 1V3V). The docking simulations indicate that Arg56 plays an important role in the binding of 15-*keto*- PGE_2 , as it has been confirmed by mutagenesis assays (Table 8). This residue establishes an interaction with the carboxylic group of the 15-*keto*- PGE_2 . Interestingly, Arg56 is replaced by Lys in other species, such as rat and pig, which show higher K_m values than human. Therefore, the presence of Arg56 may also explain the low K_m values for the human enzyme towards 15-*keto*-PGs, which have been discussed above. We have also performed mutagenesis analysis of Tyr245 in human PTGR1. Our present results

indicate the participation of this Tyr in substrate binding, although it is not absolutely required for enzyme activity. Previous site-directed mutagenesis studies with rat PTGR1³⁶ and the homologous Tyr residue (Tyr259) in human PTGR2²⁰ also give support to the non-essential role of Tyr245. In guinea-pig PTGR1, Tyr245 was hypothesized to stabilize the transition state (i.e. enolate anion) along with the 2'-hydroxyl group of the NADPH ribose²⁹. Recently, a new mechanism was proposed for an MDR enzyme belonging to the enoyl thioester reductase (ETR) family, in which a covalent adduct would be formed between the enolate anion and NADPH as a transition state intermediate⁶³. Such a catalytic mechanism would not require any amino acid residue participating in the chemical reaction, and it could be also proposed for PTGR1 and other AOR enzymes.

Despite the likely implication of PTGR1 in the PG metabolism, few works have searched for inhibitors of this enzyme. Up to date, only a preliminary screening using NSAIDs as pig PTGR1 inhibitors⁵⁴ and the structure of guinea-pig PTGR1 in complex with indomethacin have been published³⁰. Our work reports the IC₅₀ values of several NSAIDs as human PTGR1 inhibitors, showing niflumic acid and indomethacin as the best inhibitors. Both inhibitors are predicted to establish ionic interactions with Arg56 through their carboxylic acid group, as it was shown for indomethacin in the guinea-pig structure³⁰. Therefore, the carboxylic acid could be proposed as a necessary pharmacophore group in the search of new inhibitors, although the mutagenesis assays moderate the importance of Arg56. The different conformation of the Tyr262 residue between the human and guinea-pig PTGR1, along with other results from the kinetic and inhibition studies, point at differential features of the human enzyme and

thus further crystallographic studies on the human enzyme are warranted. This will facilitate the design of more selective inhibitors, which could be very useful in elucidating the role of PTGR1 in human pathologies, as it has been proposed (e.g. chemoprevention⁵⁰, tumor suppression^{46,47} and activation of antitumor drugs^{49,52}). In addition, PTGR1 inhibitors could be used to increase the physiological levels of 15-*keto*-PGE₂, which mediates the anti-proliferative response described for 15-PGDH^{64,65}, the enzyme catalyzing the previous step in the same catabolic pathway.

In summary, the present work establishes the substrate specificity of human PTGR1 with prostaglandins and α,β -unsaturated aldehydes and ketones, delineates the important active-site residues and explores the inhibitory potency of several NSAIDs against the PTGR1 activity. The inhibitors may be of interest for undertaking further studies on the enzyme mechanism and for possible pharmacological applications.

